EUROPEAN ORGANIZATION FOR NUCLEAR RESEARCH

CERN-EP/82-14
3 February 1982

SYSTEMATIC EXPERIMENTAL AND THEORETICAL STUDIES OF THE LATTICE VIBRATIONS OF HOST ATOMS AND SUBSTITUTIONAL Sn IMPURITIES IN III-V SEMICONDUCTORS

O.H. Nielsen[a)], F.K. Larsen[b)], S. Damgaard[a,c)] J.W. Petersen[a,c)], and G. Weyer[a,c)]

a) Institute of Physics, University of Aarhus, 8000 Aarhus C, Denmark.
b) Institute of Chemistry, University of Aarhus, 8000 Aarhus C, Denmark.
c) The ISOLDE Collaboration, CERN, Geneva, Switzerland.

Abstract

The lattice vibrations of the two constituent atoms in the III-V semiconductors GaP, GaAs, GaSb, InP, InAs, and InSb have been studied experimentally by neutron diffraction and theoretically by calculations within the framework of various phonon models proposed in the literature for these compounds. The mean-square amplitudes (measured at 295 K) show a general increase with increasing lattice constant and seem furthermore to reflect the partial ionicity of the compounds. The different phonon models for the lattice dynamics are compared with each other and tested critically against experimental neutron-diffraction and specific-heat data. Several models are found to be insufficient. The most satisfactory ones are some shell models.

^{119}Sn Mössbauer impurity atoms have been implanted site-selectively on the two different substitutional lattice sites and their Debye temperatures have been determined. The mass-defect model combined with an Einstein force-constant analysis is applied for a description of the impurity vibrations and an interpretation of the experimental Mössbauer data and available localized-mode data from optical experiments. Both lower and higher force constants are deduced for the impurities as compared with the host atoms. Larger force constants are found on V sites than on the III sites for Sn in the Ga compounds, whereas the opposite holds in the In compounds.

Submitted to Phys. Status Solidii (b)

SYSTEMATIC EXPERIMENTAL AND THEORETICAL STUDIES OF THE LATTICE VIBRATIONS OF HOST ATOMS AND SUBSTITUTIONAL Sn IMPURITIES IN III-V SEMICONDUCTORS

O.H. Nielsen[a)], F.K. Larsen[b)], S. Damgaard[a,c)] J.W. Petersen[a,c)], and G. Weyer[a,c)]

PACS numbers: 61.70, 63.20, 61.10, 76.80

Abstract

The lattice vibrations of the two constituent atoms in the III-V semiconductors GaP, GaAs, GaSb, InP, InAs, and InSb have been studied experimentally by neutron diffraction and theoretically by calculations within the framework of various phonon models proposed in the literature for these compounds. The mean-square amplitudes (measured at 295 K) show a general increase with increasing lattice constant and seem furthermore to reflect the partial ionicity of the compounds. The different phonon models for the lattice dynamics are compared with each other and tested critically against experimental neutron-diffraction and specific-heat data. Several models are found to be insufficient. The most satisfactory ones are some shell models.

^{119}Sn Mössbauer impurity atoms have been implanted site-selectively on the two different substitutional lattice sites and their Debye temperatures have been determined. The mass-defect model combined with an Einstein force-constant analysis is applied for a description of the impurity vibrations and an interpretation of the experimental Mössbauer data and available localized-mode data from optical experiments. Both lower and higher force constants are deduced for the impurities as compared with the host atoms. Larger force constants are found on V sites than on the III sites for Sn in the Ga compounds, whereas the opposite holds in the In compounds.

Zusammenfassung

Die Gitterschwingungen der beiden atomaren Bausteine der III-V Halbleiter GaP, GaAs, GaSb, InP, InAs und InSb wurden experimentell durch Neutronenbeugungsexperimente und theoretisch durch Rechnungen im Rahmen verschiedener in der Literatur vorgeschlagener Gitterschwingungsmodelle untersucht. Die quadratischen Mittelwerte der Schwingungsamplituden (gemessen bei 295 K) steigen insgesamt an mit steigender Gitterkonstante und zeigen darüberhinaus einen Einfluß der teilweise ionischen Bindung dieser Materialen. Verschiedene Modelle für die Gitterdynamik werden miteinander verglichen und kritisch überprüft an Neutronenbeugungsdaten und bestimmungen der specifizchen Wärme. Mehrere Modelle werden für unzureichend befunden. Am zufriedenstellindsten sind einige Schalenmodelle.

^{119}Sn Möβbauer-Fremdatome wurden substitutionell auf die beiden verschiedenen Gitterplätze implantiert durch ein Verfahren, das selektiv einen Gitterplatz auswählt, und ihre Debyetemperaturen wurden bestimmt. Für die Beschreibung der Gitterschwingungen der Fremdatome wird das Massendefektmodell kombiniert mit einer Analyse der Kraftkonstanten durch einen Einstein-Debye Ansatz. Im Rahmen dieses Ansatzes werden die Ergebnisse der Möβbauerexperimente sowie zugängliche Ergebnisse von optischen Experimenten über lokalisierte Moden interpretiert. Es werden für die Fremdatome sowohl kleinere als auch größere Kraftkonstanten verglichen mit denen des Wirtsmaterials festgestellt. Für Sn-Atome auf V Plätzen sind die Kraftkonstanten größer als auf III Plätzen in den Galliumverbindungen, während es in den Indiumverbindungen umgekehrt ist.

a) Institute of Physics, University of Aarhus, 8000 Aarhus C, Denmark.
b) Institute of Chemistry, University of Aarhus, 8000 Aarhus C, Denmark.
c) The ISOLDE Collaboration, CERN, Geneva, Switzerland.

1. INTRODUCTION

The perception that optical and electrical properties of semiconductors are influenced or even dominated by the presence of impurities has made the understanding of the role of the impurities the topic for a large number of investigations. In the past, impurities in the group IV semiconductors silicon and germanium have been studied in great detail. More recently attention has been directed towards the III-V semiconductor compounds, stimulated by their growing importance in applications such as high-frequency and opto-electronic devices[1]. Relatively few of these investigations have been devoted to direct measurements of microscopic properties of the impurities. For example, although the degree of electrical activation of a dopant species in a semiconductor is known for a large variety of conditions, the states of the impurities are in many cases actually unknown. Mössbauer spectroscopy on radioactive impurities has proved to be a powerful method, yielding direct microscopic information about the electronic structure and vibrational properties of an impurity [see, for example, Weyer et al.[2], Antoncik[3], and Petersen et al.[4]].

From a Mössbauer spectrum three parameters can be extracted[5]. Firstly, the isomer shift, which is related to the s-electron density at the Mössbauer nucleus and probes the valence electron configuration of the Mössbauer atom. Secondly, the quadrupole splitting (or broadening) of the resonance lines which is a sensitive test for non-cubic impurity surroundings and electric field gradients at the nucleus. Thirdly, the Lamb-Mössbauer factor (Debye-Waller factor, f-factor), which measures the probability of the recoilless emission/absorption of the γ-rays. The f-factor is determined by the mean-square vibrational amplitude of the Mössbauer nucleus, and gives therefore a measure of the strength of the impurity's coupling to the host lattice.

In recent years the ^{119m}Sn Mössbauer probe has been applied to study the isoelectronic Sn impurity in elemental group IV semiconductors. An understanding of such comparably simple systems is a necessary prerequisite for investigations of more complicated systems. Comparison of isomer shifts with band-structure calculations showed that the Sn valence electrons adjust to the electronic configuration of the host atoms[2,3]. Owing to the lack of sufficiently sophisticated models, the impurity vibrational properties have only recently been clarified[4,6]. An extension of Mannheim's impurity-vibration model[7] to the diamond lattice led to the conclusion that the dynamics of Sn in silicon and germanium depends sensitively on the phonon-density-of-states functions for the host lattices. These are not directly measurable, but are sufficiently well known since sophisticated phonon models became available[8]. Especially Weber's adiabatic bond-charge model[9] fits very well to experimental phonon-dispersion curves. Petersen et al.[4] tested the phonon-density-of-states functions from this model (in terms of moments of these functions) against X-ray-diffraction and specific-heat data.

A natural continuation of these studies on Sn in group IV semiconductors will be presented here, namely an investigation of the vibrational properties of Sn dopants in III-V semiconductors with the zinc-blende structure. As an amphoteric dopant, Sn occupying substitutional III and V sites acts as a donor or an acceptor, respectively. By implantations of radioactive ^{119}In and ^{119}Sb, which both decay to the Mössbauer level of ^{119}Sn, it has become possible to insert Sn atoms selectively on both III and V sites[10]. Isomer-shift measurements have shown that the electronic configurations of Sn on III and V sites are clearly distinguishable. The observed differences are basically attributed to the partly ionic character of the III-V semiconductors. (A detailed interpretation of the isomer shifts for substitutional Sn in III-V semiconductors will be published elsewhere).

Here we report on measurements of f-factors for ^{119}Sn on the III and V sites in GaP, GaAs, GaSb, InP, InAs, and InSb. An understanding of these results requires phonon models of the perfect lattices. A critical experimental test of the available phonon models is in this case more difficult than for the group IV semiconductors because the two different lattice sites have to be considered separately in order to obtain a meaningful test of a model. Specific-heat data only check the average mean-square vibrational amplitudes, whereas neutron- and X-ray-diffraction techniques can probe both lattice sites individually. However, the experimental diffraction results reported in the literature are incomplete and inconsistent in most cases. Therefore systematic neutron-diffraction measurements were performed on all six compounds to resolve the controversy. The measurements yield absolute values of the thermal mean-square amplitudes of the two atomic constituents with an accuracy of a few per cent. A critical comparison between experimental and

calculated mean-square amplitudes reveals which phonon models can be considered sufficiently accurate for the present purpose. Incidentally, this test also constitutes a way of checking phonon-polarization vectors, which have so far only been measured indirectly by Raman scattering. Inelastic neutron scattering has not yet been analysed to yield these vectors, and therefore the present test is a further check of the re ty of a phonon model.

The measured Mössbauer f-factors for Sn impurities on the two different lattice sites in the III-V semiconductors can be interpreted with the aid of reliable phonon models through the application of a model for the impurity—host lattice coupling. Models allowing mass and force-constant changes have been proposed by several authors, but owing to the complexity of the lattice dynamical description of the III-V semiconductors, in our opinion no truly satisfactory model seems to exist at present. We have therefore chosen to interpret the f-factors in terms of an Einstein-Debye description, which permits sound qualitative discussions. Furthermore, localized-vibrational-mode frequencies determined for light impurities in some of the compounds are also interpreted in the framework of the same model.

The paper is organized in the following way. In Section 2 the neutron-diffraction results together with a discussion of data from literature are presented. In Section 3 some aspects of the theory of lattice vibrations are reviewed. The phonon-model calculations are compared critically with each other and with the diffraction results of Section 2 and specific-heat data. In Section 4 the results of Mössbauer f-factor measurements for ^{119}Sn on III and V sites are given. These and the localized-mode data are interpreted by means of the simple Einstein-Debye impurity model and obtained force-constant ratios are discussed.

2. NEUTRON-DIFFRACTION DETERMINATION OF THE MEAN-SQUARE VIBRATIONAL AMPLITUDES IN GaP, GaAs, GaSb, InP, InAs, AND InSb

The aim of the neutron-diffraction study was first and foremost a consistent evaluation of the experimental data to obtain a relatively accurate set of mean-square amplitudes for the individual components in all the above listed III-V semiconductors. The values existing in the literature have quite a spread and stem from studies of varying standards. In particular, a proper correction for the effect of thermal-diffuse scattering (TDS) has not been applied in many cases. The elastic constants of the III-V semiconductors are sizeable and the omission of TDS corrections will introduce an apparent increase of the Debye-Waller parameter by $\sim 9\%$.

The Debye temperatures of these compounds are relatively low (150-400 K). Thus for room temperature studies, we anticipate the vibrations to be described adequately in the high-temperature approximation [cf. Eq. (14) below], where quantum effects are small. The validity of this assumption was tested for InSb where data were collected at 295, 373, and 473 K and the mean-square amplitudes appeared closely proportional to temperature. This observation shows furthermore that anharmonic vibrations are not substantial for InSb even at 473 K. In an accurate neutron-diffraction study on InAs and GaSb, Tibballs et al.[11] report that the anharmonic thermal parameters for these compounds are also small. Elaborate diffraction studies on other zinc-blende lattices show invariably little anharmonic effects at room temperature [e.g. ZnS[12], ZnSe[13]]. Therefore the present room temperature data sets were refined in the harmonic model.

Neutron diffraction was favoured against X-ray diffraction for this study, one reason being that for neutron diffraction the effective point scattering of the neutrons on the nuclei corresponds to the atomic neutron-scattering factors (also called scattering lengths), which are independent of the scattering angle. Thus the fall-off of intensity with increasing scattering angle is solely due to the atomic thermal motion, while for X-ray diffraction it is due to a combination of the atomic X-ray-scattering factor (also called the form factor) and the temperature factor, which increases the difficulties in the interpretation of the data. Another advantage of neutron diffraction is that the scattering lengths are very similar for all atoms in the series GaP, GaAs, GaSb, InP, InAs, and InSb, which should help to determine the mean-square amplitudes of the individual ions with comparable precision.

2.1 Neutron diffraction: experimental and data treatment

The crystals used in the neutron-diffraction measurements were slabs of GaP, GaSb, InAs, and InSb which had extended (111) faces, and since there is a pronounced cleavability along the $\{1\bar{1}0\}$ form of planes, crystal samples of equilateral triangular shape were easily prepared. The GaAs and InP slabs had extended (100) faces and a pronounced cleavability along the {110} form of planes, allowed the preparation of samples as square plates. Typical volumes of the crystal samples were 5-10 mm^3. [Detailed dimensions of the crystals are gathered along with other crystallographic data in a table which may be obtained upon request from one of the authors (F.K.L.).]

Neutron-diffraction data were collected on a four-circle diffractometer at the DR3 reactor of the Danish Research Establishment Risø. The (002) reflection from a Be monochromator crystal provided an incident neutron beam of 1.070 Å wavelength. Data collection was carried out at ambient temperature, i.e. 295 K, and for InSb at 373 K and 473 K as well. The Bragg intensities were measured with a BF_3 detector using ω-2θ step-scan technique in steps of 0.04°, over scan widths typically determined by the expression 2.5°tg θ + 2.5°.

The integrated intensities were evaluated by a method which divides the step-scanned profile into peak and background in such a way that $\sigma_{count}(I)/I$ is minimized[14]. Here I is the integrated intensity and $\sigma_{count}(I)$ its estimated standard deviation based on counting statistics.

Intensities were corrected for absorption. The linear absorption coefficients μ_{eff} for neutrons of 1.070 Å wavelength were calculated from tabulated mass-absorption coefficients and incoherent scattering cross-sections. A Gaussian grid integration[15] in 8 × 8 × 8 grid points was applied. The intensities were reduced to squared structure factors $F^2_{hkl,obs}$ by applying the inverse Lorentz factor, sin $2\theta_{hkl}$. Symmetry related reflections and remeasurements were averaged and it was observed that intensities from the extended faces tended to be relatively stronger, which is interpreted as an indication of anisotropic extinction.

The structure factors were corrected for TDS. Thermal-diffuse scattering by acoustic modes of lattice vibration peaks under the Bragg peaks and the relative contribution of the thermal inelastic scattering to the total integrated intensity (the so-called "TDS correction factor" α) increase with sin θ/λ. A correction for TDS is crucial when parameters describing the atomic vibrations are to be determined since its neglect will cause an apparent increase of the mean-square amplitude of vibration by $\Delta(u^2)$ when uncorrected integrated intensities are used. This effect can be evaluated by the approximate expression[16]

$$(1 + \alpha) = \exp\left[16\pi^2\Delta(\langle u^2\rangle)(\sin\theta/\lambda)^2\right] \tag{1}$$

The width of the plateau δ in the TDS profile can be estimated [17], and is a function of the ratio, β, between the phonon velocity and the neutron velocity, the detector aperture size, and the Bragg angle θ *(hkl)* . Except for the lowest order reflections δ was much smaller than the observed full width of the peak. Since the TDS contribution sits well inside the Bragg reflection, normal background subtraction will not correct adequately for TDS. We approximate the correction with the standard X-ray correction, and calculations for one-phonon TDS were carried out using a computer program based on work by Merisalo and Kurittu [18].

Elastic constants are found in the literature as follows:

GaP: Weil and Groves [19]
GaAs: Garland and Park [20]
GaSb: Lin and Wong [21]
InP: Hickernell and Gaytoo [22]
InAs: Burenkov et al. [23]
InSb: Slutsky and Garland [24]

2.2 Neutron diffraction: refinements

The nuclear structure factor F_{hkl} is a function of the scattering vector $\vec{Q} = 2\pi\vec{H}$, where $\vec{H}$ is the reciprocal lattice vector

$$\vec{H} = h\vec{a}_1^* + k\vec{a}_2^* + l\vec{a}_3^* \tag{2}$$

and the reciprocal lattice vectors $\vec{a}_j^*$ are related to the vectors $\vec{a}_i$ of the direct unit cell by

$$\vec{a}_i \cdot \vec{a}_j^* = \delta_{ij} \quad . \tag{3}$$

The expression for the structure factor is

$$F_{hkl}(\vec{Q}) = \sum_j b_j \exp\left(i\vec{Q} \cdot \vec{r}_j\right) \exp\left(-1/2Q^2\langle u^2\rangle_j\right) \quad . \tag{4}$$

Here b_j is the nuclear scattering-amplitudeof the atom located at the equilibrium position $\vec{r}_j$ in the unit cell. The thermal vibrations expressed as mean-square amplitudes are taken into account by the second exponential function, the temperature factor, which is the square root of the Debye-Waller factor. The III-V compounds with a zinc-blende lattice are described in the cubic space group, F $\bar{4}$3m, with the cation (Ga or In) located at the origin site and the anion (P, As or Sb) at (1/4,1/4,1/4).

The nuclear scattering-amplitudes were taken from Bacon[25] except for b_{As} and b_{Sb}[11]. The parameters of the structure factors were refined in a least-squares procedure, minimizing the expression

$$\sum_{hkl} w \left(F_{obs}^2 / E_{hkl(g)} k^2 F_{calc}^2\right)^2 \quad . \tag{5}$$

with weights $w = 1/(\sigma_{count} + 0.02\, F_{obs}^2)^2$. Here $E_{hkl(g)}$ is the extinction coefficient, which was taken to be a function of a single isotropic extinction parameter g. k is a scale factor, and the summation is over all sets of observed and calculated structure factors F_{obs}, F_{calc}. The structure factors of each compound are thus described with only four parameters, namely a scale factor parameter k, an extinction parameter g, and mean-square amplitudes for the atoms at the two sites $\langle u^2\rangle_{III}$, and $\langle u^2\rangle_V$, respectively.

The stronger intensities observed for all crystals were moderately to heavily influenced by extinction. A correction for isotropic extinction following the theory of Becker and Coppens [26] was applied. With all atoms parameters tended to be quite correlated, so a careful strategy in the refinements was strived for. The intensities of the zinc-blende lattice fall into three groups as expressed for InP:

$$\begin{aligned} F_{hkl}^2 = 16[b_{In}T_{In} + b_P T_P]^2 \quad & \text{for } h+k+l = 4n \\ 16[b_{In}^2 T_{In}^2 + b_P^2 T_P^2] \quad & \text{for } h+k+l = 4n+1 \\ 16[b_{In}T_{In} - b_P T_P]^2 \quad & \text{for } h+k+l = 4n+2. \end{aligned} \tag{6}$$

The scattering lengths of all atoms in this group of III-V compounds are very similar, which means that the group of structure factors with $h + k + l$ an odd multiple of 2 are quite weak. This group of weak reflections for each structure was used to determine an approximate value of the scale factor under the assumptions that extinction was negligible and that the intensities of the low-order weak reflections are insensitive to the value of the Debye-Waller factor parameter. As a next step the group of medium-strong intensities was included in the refinement of the two thermal parameters and an isotropic extinction parameter, for the scale factor fixed at a value determined by the weak reflections. For most of the compounds all four parameters thereafter remained stable with little change of scale factors relative to the value determined by the weak intensities alone, even when all reflections were included in the refinements. Obviously the extinction for all crystals was anisotropic—with [111] constituting an extreme direction—but the data material was not extensive enough to allow for a refinement procedure with an anisotropic extinction model. It was therefore chosen to exclude the lowest order, most heavily extinct intensities from the refinements, and satisfactory convergence was obtained in all cases for an isotropic extinction model. Results of the refinements are included in Table 1. [More detailed information on the refinements as well as lists of the observed and calculated structure factors may be obtained from one of the authors (F.K.L.).]

2.3 Discussion

Table 1 is a compilation of experimental values for the mean-square amplitudes of the III-V semiconductors GaP, GaAs, GaSb, InP, InAs, and InSb. Close examination of Table 1 shows that the present neutron values are in fair agreement with the values from the most reliable determinations and may be considered the more accurate estimates except in the cases of InAs and GaSb, which recently have been studied in more detail by Tibballs et al. [11]

The whole series of compounds was investigated by X-ray diffraction by Shumskii et al. [28]. They report mean-square amplitudes as a function of temperature. However, for a given temperature the analysis for each compound was based on only six intensities. Their values for mean-square amplitudes show marked deviations from proportionality with temperature at quite moderate temperatures, e.g. for InSb starting at 400 K and for InAs at 300 K. No such appreciable deviation was observed for InSb up to 500 K in the present study, and also Tibballs et al.[11] report much less deviation for InAs. The room-temperature values of Ref. 28 agree generally better with the neutron results, and the relative trend through the series of III-V through the series of III-V compounds is the same.

Figure 1 shows the mean-square amplitudes of the single-crystal neutron studies plotted as a function of the unit-cell dimension (i.e. as a function of increasing interatomic distance). Clearly, as a general trend the average atomic mean-square amplitude increases with increasing interatomic distance. A qualitative explanation for this correlation might be that the compounds crystallizing with a rather large atomic separation [corresponding to a minimum in the total energy, see Yin and Cohen [37]] consequently have less overlap of the valence electrons. It may be reasonable to assume that this leads to a softer interatomic bonding and hence to a larger mean-square amplitude. The amplitudes of the group IV semiconductors Si, Ge, and α-Sn [38] follow the same trend, but fall lower than those of the III-V compounds with similar lattice constants (cf. Fig. 1). For the group IV elements this trend has been found to correlate with a dehybridization of the covalent bonds[2]. The differences between group IV and III-V semiconductors may be seen as an indication of the partially ionic character of the III-V bonds. Experimental bond-charge determinations for GaSb [39] and InSb [35] are characteristic of partly ionic and partly covalent bonds. Furthermore, band-structure calculations[40,41] show charge transfer from the anion to the cation, giving rise to bond ionicity. Thus from Fig. 1 a softening of the bonds due to ionicity is indicated, since the average $\langle u^2 \rangle$ for the compounds with the highest ionicity (InP, GaP) tends to deviate the most from the line given by the three covalent semiconductors.

Figure 1 shows furthermore that the vibrational amplitudes of the cation is larger than that of the anion for InP, InAs, and InSb. This is in accordance with the findings in a number of the more elaborate diffraction studies on zinc-blende compounds, e.g. InAs [11], GaSb [11], ZnS [12], ZnSe [13], and ZnTe [42].

It appears that for GaP, GaAs, and GaSb the mean-square amplitude of the cation might be smaller than that of the anion. However, for GaP and GaSb the mean-square amplitudes are almost identical for the two ions and the GaAs refinements were plagued with considerable parameter correlations. A careful study[11] of GaSb contradicts our findings, so a decision on whether the Ga compounds constitute a special case must await further more accurate diffraction studies.

3. LATTICE VIBRATIONS IN III-V SEMICONDUCTORS

3.1 Theory of lattice vibrations

The general theory of thermal vibrations is briefly reviewed as far as it is relevant for the study of the mean-square amplitudes of the atomic constituents of the III-V compounds. Using the notation of Maradudin et al. [43], the harmonic vibrational Hamiltonian is given by

$$H = \sum_{l\kappa} \frac{\vec{p}(l\kappa)^2}{2M_\kappa} + \frac{1}{2} \sum_{\substack{l\kappa, \\ l'\kappa'}} \vec{u}(l\kappa) \bar{\bar{\phi}}(l\kappa, l'\kappa') \vec{u}(l'\kappa') \quad , \tag{7}$$

where l denotes the unit cells and κ the atoms therein. $\vec{u}$ and $\vec{p}$ are displacement and momentum operators, M_κ the atomic masses and $\bar{\bar{\phi}}(\ell\kappa, \ell'\kappa')$ the harmonic force-constant matrix between atoms $e\kappa$ and $e'\kappa'$. The eigenfunctions of H are phonon frequencies ω^2. The number of phonon frequencies in the interval $[\omega; \omega + d\omega]$ is the **phonon-density-of-states** function $g(\omega)$ times $d\omega$. Formally $g(\omega)$ may be expressed as

$$g(\omega) = \frac{1}{N} \sum_{j=\text{phonons}} \delta(\omega - \omega_j) \quad . \tag{8}$$

The sum has for convenience been divided by the number of phonon degrees of freedom N so that $g(\omega)$ has unit integral.

When a lattice contains different atoms in the unit cell, the atomic displacements $\vec{u}(\ell\kappa)$ differ according to the phonon-polarization vector $\vec{w}$ of a given phonon,

$$\vec{u}(\ell\kappa) = \frac{1}{\sqrt{M_\kappa}} \vec{w}(\kappa \mid \vec{k}j)\, e^{i\vec{k}\cdot\vec{x}(\ell)-i\omega_j(\vec{k})t} \quad . \tag{9}$$

Here $\vec{k}$ is the phonon wave vector and j its band index. We now introduce the **lattice-site vibrational density-of-states,** which refers to a given atom κ in the unit cell (e.g. the III site or the V site) and space direction by

$$g_{\kappa_\alpha}(\omega) = \frac{1}{N}\sum_{\vec{k}j} \mid \vec{w}_\alpha(\kappa \mid \vec{k}j) \mid^2 \delta\left(\omega - \omega_j(\vec{k})\right) \quad . \tag{10}$$

The sum is weighted by the polarization vectors, and is over the first Brillouin zone and all phonon bands. Division by the number of unit cells N assures that the integral of $g_{\kappa\alpha}(\omega)$ is unity [by Eq. (2.1.61b) of Ref. 43]. In the case of a III-V compound the phonon density-of-states, Eq. (8), is also given by

$$g(\omega) = \frac{1}{2}g_{III}(\omega) + \frac{1}{2}g_V(\omega) \quad , \tag{11}$$

where III and V refer to the two lattice sites, and α is arbitrary in a cubic lattice.

The phonon- or the site-density-of-states functions are unfortunately not directly measurable. Experimental quantities can nevertheless be expressed in terms of one or more weighted moments of these functions [44]. The moments are conveniently expressed in terms of Debye temperatures[45]

$$\theta_D(n) = \frac{\hbar}{k_B}\left(\frac{n+3}{3}\int_0^{\omega_{\max}} \omega^n g(\omega)\, d\omega\right)^{1/n} \quad . \tag{12}$$

$n \geq -3$ is the power of ω weighting the $g(\omega)$ function.

An example is the mean-square vibrational amplitude of, for example, the site III atoms given by the general expression

$$\langle u_x(III)^2\rangle = \frac{\hbar}{2M_{III}}\int_0^{\omega_{\max}} \frac{1}{\omega} g_{III}(\omega) \coth\left(\frac{1}{2}\hbar\omega/k_BT\right) d\omega \tag{13}$$

[cf. Eq. (2.4.24) of Ref. 43]. For high temperature ($k_B T > \hbar\omega_{max}/2\pi$) the coth-factor can be expanded in a power series. In terms of Debye temperatures we find

$$\langle u_x(III)^2\rangle = \frac{3k_BT}{M_{III}}\left[\frac{\hbar}{k_B\theta_D(-2)_{III}}\right]^2\left[1 + \left(\frac{\theta_D(-2)_{III}}{6T}\right)^2 - \left(\frac{\theta_D(-2)_{III}\theta_D(+2)_{III}}{60T^2}\right)^2 + \cdots\right] \quad , \tag{14}$$

where $\theta_D(n)_{III}$ corresponds to the $g_{III}(\omega)$ function. Only the leading term is needed when $T \gg 1/6\,\theta_D(-2)_{III}$ making $\langle u_x(III)^2\rangle$ linear in T. At Tclose to zero, Eq. (13) becomes with the aid of Eq. (7.2.25) of Ref. 43:

$$\langle u_x(III)^2\rangle_0 = \frac{3}{4}\frac{\hbar^2}{M_{III}k_B\theta_D(-1)_{III}}\left[1 + \frac{2}{3}\pi^2\frac{\theta_D(-1)_{III}}{\theta_D(-3)_{III}}\left(\frac{T}{\theta_D(-3)_{III}}\right)^2 + \cdots\right] \quad . \tag{15}$$

We see that measurements of site III vibrational amplitudes can yield essentially two Debye temperatures $\theta_D(-2)_{III}$ and $\theta_D(-1)_{III}$.

Another example where moments of the density-of-states function can be obtained from experiment is the lattice heat-capacity. The harmonic c_V is (per unit cell)

$$c_V(T) = 3rk_B \int_0^{\omega_{\max}} \left(\frac{\hbar\omega}{2k_BT}\right)^2 \sinh\left(\frac{\hbar\omega}{2k_BT}\right)^{-2} g(\omega)\, d\omega \quad , \tag{16}$$

where r is the number of atoms in the unit cell [Eq. (4.1.7) of Ref.43]. Measurements of $c_V(T)$ are usually presented in terms of a temperature-dependent Debye temperature $\theta_D(T)$. Going one step further, Barron et al.[46] showed how these data can be analysed to obtain the $\theta_D(n)$ for $g(\omega)$. For example, it is found that in fact $\theta_D(T \to \infty) = (\theta_D n = 2)$ and $\theta_D(T = 0) = \theta_D(n = -3)$. The moments for $n = [-3;0],1,2,4,6$ can be obtained by a careful analysis, provided accurate $c_V(T)$ data exist down to $T \simeq 1$ K. This allows for a critical test of the phonon-density-of-states function. The site density-of-states [e.g. $g_{III}(\omega)$ and $g_V(\omega)$] cannot be probed, however, since $c_V(T)$ is given by the sum of these functions, cf. Eq. (11).

It should be emphasized that a comparison of different experiments and phonon models concerning temperature-dependent quantities like the above mentioned, can **only** be performed in terms of the different $\theta_D(n)$. The often displayed $\theta_D(T)$ curves from experiments or models convey only very limited information about other physical quantities.

3.2 Phonon-density-of-states calculations

Several phonon models for III-V semiconductors based on different assumptions about the interatomic forces have been put forward[8]. The reliability of the density-of-states functions derived from the available models will be judged pragmatically in the following from their ability to describe various experimental data, and no discussion of the physical basis of the models will be given. We have considered only those models which include the important long-range Coulomb forces, namely the shell model[47,48] (SM), the deformable-ion model[49] (DIM), the deformation-dipole model[50] (DDM) and the rigid-ion model[50] (RIM). Recent SM fits were presented by Borcherds and Kunc[51] for InP, InAs, and InSb, and by Borcherds et al.[52] for GaP. Vibrational amplitudes in all III-V semiconductors were calculated by Vetelino et al.[53] using a simple RIM fitted to the elastic constants. Also, Talwar and Agrawal[54] presented calculations. Since then more complete phonon-dispersion data have become available, and a more accurate analysis is warranted. Systematic zinc-blende structure Debye-Waller factors have very recently been calculated by Reid[55].

The phonon-model programs of Kunc and Nielsen[56] and Nielsen and Jaswal[57] were employed for the density-of-states calculations. Methods for obtaining phonon-density-of-states functions were reviewed by Gilat[58]. However, we applied the recent hybrid-tetrahedron scheme of MacDonald et al.[59]. This permits quadratic interpolation of both frequencies and weight factors in $\vec{k}$-space [cf. Eq. (10)]. With 105 $\vec{k}$-vectors the irreducible Brillouin zone was divided into 2560 small tetrahedra, and the $g_{III}(\omega)$ and $g_V(\omega)$ functions were calculated. From these we derived the $\theta_D(n)_{III}$, $\theta_D(n)_V$, and $\theta_D(n)$ Debye temperatures given in Tables 2–7. Comparing with several calculations using 22720 tetrahedra, we believe the θ_D to be accurate to about 1% for a given model.

3.3 Analysis of heat-capacity data

Measurements of $c_V(T)$ for III-V semiconductors were performed by Piesbergen[65], Cetas et al.[66] Tarassov and Demidenko[62], and Irwin and La Combe[63]. For GaP and InP no low temperature ($\sim$ 1 K) data exist. An analysis of these data sets was performed using the method of Barron et al.[46] to obtain the $\theta_D(n)$. The errors on $\theta_D(n = 2,4,6)$ are estimated from the fitting procedure. For the remaining $\theta_D(n)$ the errors should be below $\sim$ 1 K, but there is still the possibility of systematic errors in the data[66,70]. The results are given in Tables 2–7.

3.4 Comparison of results from models and experiments

Any comparison of phonon models with thermal quantities [e.g. $\langle u^2 \rangle$ or $c_V(T)$] should be performed as argued above by means of weighted moments of the density-of-states functions[44], most conveniently

expressed in terms of Debye temperatures $\theta_D(n)$. The X-ray and neutron-diffraction results of Section 2 were converted to Debye temperatures by means of the expansion in Eq. (14), since the high-temperature expansion was always valid. The average Debye temperature $\theta_D(-2)$ of the $g(\omega)$-function is found from Eqs. (11) and (12) to be

$$\frac{2}{\theta_D(-2)^2} = \frac{1}{\theta_D(-2)^2_{III}} + \frac{1}{\theta_D(-2)^2_V} \quad . \tag{17}$$

These results are given in Tables 2–7 together with the model results of Section 3.2. The comparison deals with all the six III-V semiconductors separately.

3.4.1 GaP

The five models differ drastically on $\theta_D(n)_{III,V}$, although they agree well on $\theta_D(n)$ and with specific heat $\theta_D(n)$. The differences are due to disagreement about phonon-polarization eigenvectors, whereas the phonon frequencies are fairly realistic. The neutron-diffraction θ_D are all slightly low, indicating that the measured $\langle u_x^2 \rangle$ may be too large. Nevertheless, the 14-parameter SM of Yarnell et al.[61] is considered the most reliable one, especially when comparing ratios $\theta_D(-2)_{III}/\theta_D(-2)_V$.

3.4.2 GaAs

The neutron and specific-heat data agree reasonably. Drastic differences in the $\theta_D(n)_{III,V}$ are found between the seven models, but as for GaP the results for $\theta_D(n)$ agree between the models and with specific-heat data. Comparing the models with neutron-diffraction data shows that the SMs *Bii* and *Cii* of Dolling and Waugh[64] give good fits. The DDM, RIM, and the remaining SMs appear less realistic. The most convincing models are thus the two 14-parameter SMs[64].

3.4.3 GaSb

The two neutron-diffraction results agree reasonably with each other and with specific-heat data. The model values for $\theta_D(n)_{III,V}$ differ by up to some 15%, whereas the $\theta_D(n)$ again are consistent and agree fairly well with specific-heat $\theta_D(n)$. Comparing with experimental data the valence-shell model of Kunc and Bilz[60] appears most accurate, whereas the SM[67] is perhaps acceptable, and the RIM[68] unrealistic.

3.4.4 InP

The neutron-diffraction results agree well with specific-heat data. The SM[51] and RIM[68] θ_D differ by up to 10%. The SM agrees well with specific-heat data and neutron $\theta_D(-2)_{III}$, whereas it is unrealistic for $\theta_D(-2)_V$. Perhaps a different fit would improve the situation. The RIM is altogether unrealistic.

3.4.5 InAs

for InAs no inelastic neutron-scattering determination of the phonon dispersion exists so far. The $\vec{k} = \vec{0}$ optical modes have been measured, however. Borcherds and Kunc[51] interpolated InAs between InP and InSb and suggested two valence-shell-model parameter sets.

The two neutron-diffraction results agree well with each other and with specific-heat data. The two models are also consistent with each other and with specific-heat data. The models predict $\theta_D(-2)_{III}$ well, but as for InP there is no agreement on $\theta_D(-2)_V$. If a good SM fit for InP were obtained, this problem would probably be resolved by a new interpolation procedure. Nevertheless it would be extremely useful to measure the phonon dispersion of InAs by inelastic neutron scattering.

3.4.6 InSb

The neutron data show good agreement with specific-heat data. Again drastic differences between the model $\theta_D(-2)_{III,V}$ are found, although relatively good agreement is seen for $\theta_D(n)$. The diffraction data are fitted well by the 14-parameter SM model of Price et al.[69], whereas the DDM[50], SM[51], and RIM[50] all are unrealistic. The DIM[49] also gives a good fit to the diffraction data.

From this detailed comparison it is concluded that several phonon-model fits are inadequate for a description of atomic vibrational amplitudes. These amplitudes are dominated by the long-wavelength acoustical phonons and their polarization vectors, so the inadequacy applies mainly to these. In fact, it is

possible that the optical phonons may still be well described by some of the models. It was found that several models could fit the heat-capacity Debye temperatures $\theta_D(n)$, but when the phonon-polarization vectors were checked against $\theta_D(-2)_{III,V}$ from neutron diffraction, some models were deficient. The DDM and the RIM did not give realistic results in any of the III-V semiconductors. It is doubtful whether their model assumptions are physically satisfactory, but in this connection it would be interesting to extend the DIM of Jaswal[49], which works well for InSb, to all the III-V compounds.

On the other hand, a model's failure in the present comparison does not necessarily imply a complete lack of physical realism. It was found that more or less similar SMs gave somewhat different results, and this is to some extent due to different philosophies applied in fitting the phonon model to the available data. Since our comparison is sensitive to the low-frequency phonons, a model fit that does not properly describe the elastic constants is likely to come out as inaccurate. This appears to be the case[71] with the SMs of Kunc and Bilz[60].

Another problem is associated with the fitting of a many-parameter ($\sim$10–15) model to phonon-dispersion data. It may be difficult or even impossible to find a unique minimum in the least-squares sum due to extreme parameter correlations, and "physical" considerations are often applied. Thereby a parameter set may be "forced" in such a way that, for example, the phonon-polarization vectors become unrealistic. This point could be checked in future model fits by performing the above comparison with neutron-diffraction data.

In conclusion, we find that for four of the six III-V semiconductors it is possible to find acceptable SMs for the phonons. Good models for InP and InAs are still lacking, as are phonon-dispersion data for InAs. However, realistic Debye temperatures $\theta_D(-2)_{III}$ and $\theta_D(-2)_V$ for the atomic vibrational amplitudes are given from the neutron-diffraction experiments. Even though we have reviewed many of the best phonon models known today, it would be interesting to perform a **systematic** fitting of all six compounds using, for example, a particular version of the SM, and **one** philosophy of fitting (like an unconstrained χ^2-fit). A good fitting program would also yield parameter standard deviations and intercorrelations, which unfortunately have never been indicated in the published model fits.

4. IMPURITY VIBRATIONS IN III-V SEMICONDUCTORS

4.1 Theory of impurity vibrations

The theory of lattice dynamics for perfect crystalline materials has in the last two decades reached a high degree of sophistication. In consequence, progress has also been achieved on the lattice dynamics of impurities embedded in host materials. The formalism of this problem is well known, employing the Green's function method described by, for example, Maradudin et al.[43]. Both local changes of masses and force constants can be taken into account in this framework. However, the impurity vibration models are scarce and the models only rarely reach the level of sophistication of the best corresponding models for the perfect lattice phonons. The reason for the limited theoretical effort may be found in the fact that the impurity vibrations represent very localized and microscopic properties, which are difficult to measure. However, the thermal mean-square amplitudes of impurities can be determined by Mössbauer spectroscopy.

The probability of recoilless γ-emission or absorption from a Mössbauer atom embedded in a host lattice is given by the expression[72]

$$f = \exp\left(-\vec{k}_\gamma^{\,2}\langle u_x'^2\rangle\right) \tag{18}$$

(the Lamb–Mössbauer factor, or Debye–Waller factor, or f-factor) where $\vec{k}_\gamma$ is the γ-ray wave vector R and $\langle u_x'^2\rangle$ is the thermal vibrational amplitude of the Mössbauer atom. This formula holds for an impurity of cubic symmetry. Since the f-factor is given by $\langle u_x'^2\rangle$, it depends on the details of the bonding of the Mössbauer atom to the host lattice[4,44]. In analogy with Eq. (14) the high-temperature expression for the f-factor is, within the harmonic approximation,

$$f = \exp\left[-\frac{6E_R T}{k_B \theta'_D(-2)^2}\left(1+\left(\frac{\theta'_D(-2)}{6T}\right)^2 - \ldots\right)\right] \quad , \tag{19}$$

where only the leading term is needed when $T \gg 1/6\,\theta'_D(-2)$. Here T is the temperature, E_R the recoil energy of the emitting/absorbing Mössbauer nucleus, and $\theta'_D(-2)$ is the impurity Debye temperature, which is rigorously defined as for the perfect lattice in Section 3 (see also Ref. 6).

If the Mössbauer impurity atom is asumed to be an isotopic mass defect with no force-constant changes, it is found (cf., for example, Ref. 4) that

$$\theta'_D(-2) = \sqrt{\frac{M}{M'}}\,\theta_D(-2) \quad , \tag{20}$$

where M' is the impurity mass. $M$is the mass and $\theta_D(-2)$ the Debye temperature (Section 3) of the substituted atom. In the more general case the impurity force constants are changed, which is indicated experimentally by a deviation from Eq. (20). Nielsen[6] showed that **any** impurity model will give

$$\theta'_D(-2) = \sqrt{\frac{M}{M'}}\,\theta_D(-2) F(\bar{\bar{G}};\overline{\Delta\phi}) \quad , \tag{21}$$

i.e. the mass-defect result multiplied by an unknown function F (of order unity) of the force-constant changes $\Delta\bar{\bar{\phi}}$ and the perfect-lattice Green's function $\bar{\bar{G}}$.

Several models of force-constant changes have been proposed which could be used to calculate F. The Einstein–Debye model[44], an empirical first guess, yields

$$F(\bar{\bar{G}};\overline{\Delta\phi}) = \sqrt{\frac{\phi'}{\phi}} \quad , \tag{22}$$

where ϕ and ϕ' are "typical" force constants in the perfect lattice and around the impurity, respectively. This model is useful only for qualitative discussions. On the other hand, an Einstein–Debye force-constant ratio ϕ'/ϕ displays the value of F, and therefore ϕ'/ϕhas a well-defined meaning.

The only analytical microscopic model is due to Mannheim and co-workers[6] (see also Refs. 4, 44, and 73). It assumes nearest-neighbour central forces (making, for example, the zinc-blende lattice unstable). In the Appendix it is shown that for zinc-blende lattices the following simple formula also holds:

$$F(\bar{\bar{G}};\overline{\Delta\phi}) = \left[1 + \frac{5}{9}\left(\frac{\theta_D(-2)}{\theta_D(+2)}\right)^2\left(\frac{\phi}{\phi'} - 1\right)\right]^{-1/2} \quad , \tag{23}$$

$\theta_D(n)$ are the Debye temperatures of the perfect lattice atom that has been substituted.

The more sophisticated phonon-model concepts have so far only been used to describe isovalent impurities in group IV semiconductors[6].

Another experimental method, widely used to investigate impurity properties, is infrared or Raman determination of localized-mode frequencies. These modes exist for light and/or strongly bound impurities, whose typical frequencies consequently lie above the phonon bands. Therefore the modes have amplitudes that decay exponentially away from the impurity site. The theoretical treatment of these modes may be found, for example, in Ref. 43. We summarize here the results of the simple isotopic mass-defect model. Dawber and Elliott[74] showed that the condition for the occurrence of a localized or gap made at $\omega = \omega_L$ is

$$1 - \varepsilon\omega_L^2 \int_0^\infty \frac{g(\omega')}{\omega_L^2 - \omega'^2} d\omega' = 0; \quad g(\omega_L) \equiv 0 \quad . \tag{24}$$

Here $g(\omega)$ is an appropriate density-of-states function [in the present context $g_{III}(\omega)$ or $g_V(\omega)$], and $\varepsilon = (M - M')/M$.

In the analysis of experiments force-constant changes have to be taken into account. In the first qualitative analysis we propose to use the Einstein-model picture in the following sense. If ω_{exp} is the experimentally determined mode frequency, and ω_{MD} is the mass-defect-model prediction from a realistic density-of-states function, we define an Einstein force-constant ratio ϕ'/ϕ by

$$\omega_{exp} = \omega_{MD}\sqrt{\phi'/\phi} \tag{25}$$

It is also possible to apply the model of Mannheim[6] for obtaining force-constant ratios. The condition for a localized mode ω_L is given for diamond lattices by, for example, Petersen et al.[4], and for zinc-blende lattices the condition is discussed in the Appendix.

In the final step sophisticated phonon-model concepts should be applied for localized-mode frequencies. The RIM has been used for this purpose [see Vandevyer et al.[75] and references cited therein], changing among the many force-constant parameters only the (important) nearest-neighbour central force of the substitutional impurity. Nielsen[6] calculated localized modes of light impurities in group IV semiconductors using an adiabatic bond-charge model.

It was shown in Section 3, however, that only a subset of the available III-V semiconductor phonon models could be considered sufficiently accurate, particularly at low phonon frequencies. An unrealistic behaviour in this range may influence the higher frequency parts of the density-of-states functions, since the functions are all normalized to unit area. Thus doubt is cast on localized-mode frequencies calculated from certain models, particularly all the RIMs. Even if a realistic phonon model is chosen for the perfect lattice, a consistent approach to impurity properties should change all the forces connected with the impurity. Here the long-range Coulomb forces present a problem, which was however solved by Page and co-workers[76]. The numerical solution of the problem has thus become a formidable task, and since the phonon models need a systematic reconsideration to improve their accuracy, we believe that the sophisticated impurity models are unfeasible as yet for the III-V semiconductors.

4.2 Mössbauer measurements

4.2.1 Sample preparation

If Sn is incorporated during the crystal growth or by diffusion into III-V semiconductors, a preferential occupation of the III site is observed [see references cited in Petersen et al.[77]]. This behaviour has recently been found to hold also for ion-implanted Sn[77,78]. Thus for a selective incorporation of Sn on III or V sites, a special technique has been utilized. The technique consists of an implantation of radioactive precursors to the element ^{119}Sn, namely ^{119}In and ^{119}Sb, which both decay to the 24 keV Mössbauer level of ^{119}Sn. With an appropriate choice of implantation temperature and/or annealing temperature, ^{119}In preferentially occupies III sites, whereas ^{119}Sb is localized on V sites. After the radioactive decays the properties of ^{119}Sn on the two different lattice sites are studied by Mössbauer emission spectroscopy.

Radioactive $^{119}Sb^+$ ions were implanted either at room temperature or at 300–350°C at an energy of 80 keV to a total dose of $\sim 10^{13}$ atoms/cm^2 with an isotope separator. The ^{119}Sb activity was obtained from a bombardment of natural tin with 20 MeV α-particles by a procedure described previously[79]. The radioactive $^{119}In^+$ ions were obtained as proton-induced fission products in a uranium-carbide target irradiated with 600 MeV protons from the CERN Synchro-cyclotron. Following on-line mass separation in the ISOLDE mass separator [80,81], the 60 keV ions were implanted to a total dose of $\sim 10^{11}$ions/cm^2. Room temperature implanted samples were annealed at temperatures up to 400°C either in a dry-nitrogen flow or in a silicone-oil bath.

4.2.2 Mössbauer set-up

The Mössbauer γ-rays from the relatively weak ^{119}Sb sources ($\sim$ 5 μCi, $T_{\frac{1}{2}}$ = 38 h) and the strong short-lived ^{119}In sources ($\sim$ 10 mCi, $T_{\frac{1}{2}}$ = 2.1 min) were detected with fast resonance counters of the parallel-plate avalanche counter type [82] equipped with $CaSnO_3$ electrodes. The counters were mounted on conventional drive systems connected to a multichannel analyser or an on-line computer system operating in the multiscaling mode. The ^{119}Sb sources could be cooled in conventional cryostats for measurements at

77 K. The ^{119}In sources, owing to their short half-life, had to be dropped in an open cryostat into liquid nitrogen. In these circumstances the temperature of some samples may have been slightly higher than 77 K at the beginning of the measurement.

4.2.3 Results and data analysis

A number of Mössbauer spectra from implantations of ^{119}In and ^{119}Sb in some of the six III-V compounds are given in Refs. 10, 83, and 84. In all cases for room-temperature implantations Mössbauer lines characteristic of complex defects were found apart from lines due to substitutional Sn. A more detailed discussion of the annealing of the implantation-induced complex defects will be given elsewhere. Here we give two representative examples. Figure 2 shows spectra of ^{119}In implanted at room temperature into GaSb. Both spectra were recorded at a source temperature of 300 K, a) as implanted, and b) after an annealing of the sample at 200°C. The spectra have been fitted with two Lorentzian lines. Line 1, which is growing upon annealing, is the substitutional line, whereas line 2, which decreases upon annealing, stems from an Sn impurity-vacancy complex. Figure 3 displays a spectrum recorded at 300 K for ^{119}Sb implanted at 325° into GaSb. The spectrum has been fitted with a single Lorentzian line (the substitutional line) demonstrating that no complex defects are formed during the hot implantation. The spectra from room temperature implantations of ^{119}In into GaP[83], GaAs[85], and InP[10,84] show lines from complex defects with large intensities, whereas in InAs and InSb only low intensities are found in the defect lines. It was possible in all cases to reduce the intensity of the lines from complex defects by annealing procedures so much that reliable Debye temperatures for the substitutional sites could be determined.

For an ideal single line in a Mössbauer spectrum the area is defined as[4]

$$A^* = \int_{-v_{max}}^{v_{max}} \frac{n(v) - n(\infty)}{n(\infty)} dv \quad , \tag{26}$$

where $[-v_{max}; v_{max}]$ is the velocity range scanned. It can be shown that in this case (well-defined measuring temperatures, large source strengths, and no residual intensities in defect lines) the uncertainty in the determination of A* is 2–3%. In some of the measurements described here these requirements have not been completely fulfilled, so the uncertainties may be larger. In those cases the given uncertainties include the systematic errors in the measurements.

The following relation[4] holds for the relative areas and Debye–Waller factors measured at temperatures T_1 and T_2

$$\frac{A^*(T_2)}{A^*(T_1)} = \frac{f(T_2)}{f(T_1)} \quad . \tag{27}$$

The high-temperature expansion Eq. (19) may then be applied to Eq. (27). From a measurement of A* at two temperatures (here 77 K and 300 K) the impurity Debye temperature $\theta'_D(-2)$ can therefore be determined. The Debye temperatures found for Sn on V sites are listed in Table 8 [the values given here deviate slightly from previously published values that were based on less extensive experimental data[84,85]].

The Debye temperatures for Sn on III sites derived by this method were found to be rather inaccurate owing to some irreproducibility of the 77 K measurements following ^{119}In implantations. This apparently stems from the cooling problem discussed in Section 4.2.2. For these data a different and more accurate analysis was therefore performed. Room temperature spectra were measured in a sequence with the same resonance counter, and areas for different materials — among them silicon — immediately relate the relative Debye–Waller factors through[4]

$$\frac{A^*_1(T)}{A^*_2(T)} = \frac{f_1(T)}{f_2(T)} \quad , \tag{28}$$

where 1 and 2 refer to two different materials. Since the Debye temperature for ^{119}Sn in silicon is known very accurately[4] [$\theta'_D(-2) = 223(4)$ K] the $\theta'_D(-2)$ for ^{119}Sn on III sites in the III-V semiconductors can be

extracted with good accuracy (Table 8). Within error bars these $\theta'_D(-2)$ were found to agree with the less accurate results obtained using Eq. (27). The $\theta'_D(-2)$ are displayed in Fig. 4.

Table 8 also lists the isomer shifts for the substitutional III and V sites, demonstrating that by this parameter the two sites can be clearly distinguished (see Refs. 77 and 78 for details). Furthermore, lists of the Debye temperatures $\theta'_D(-2)_{MD}$ predicted from the mass defect model [cf. Eq. (20)], the Einstein-Debye force-constant ratios $(\phi'/\phi)_{ED}$ [cf. Eq. (22)], and the Mannheim-model force-constant ratios $(\phi'/\phi)_M$[cf. Eq. (23)] are given. In Eq. (23) the model values for $\theta_D(\pm 2)$ from Tables 2–7 were used, whereas with Eq. (21) the experimentally determined $\theta_D(-2)$ were applied.

4.3 Localized-mode data

The localized modes of light impurities in semiconductors, discussed in Section 4.1, have been the subject of many experimental investigations, especially for Si, Ge, GaP, and GaAs host crystals. The impurities, usually having masses of ~ 6–30 amu, have mainly been investigated by optical techniques, and the methods and results have been extensively reviewed by Barker and Sievers[86]. Since 1975 to our knowledge localized mode data in III-V semiconductors have only been published for InP [87,88].

We have calculated the localized mode frequencies using the mass-defect model [Eq. (24)] for B, C, Al, Si, P, Ga, and As impurities in all six III-V semiconductors. All phonon models from Section 3 were employed, but the extensive results are not presented. It was found that the localized-mode frequency of an impurity on a given lattice site could vary by up to 20% when using different phonon models with Eq. (24). Conclusions on force-constant ratios from either simple [Eq. (25)] or more complicated[75] models should therefore be considered with care. In the present work we have selected the phonon models that were favoured in the tests of Section 3. In this way it is hoped that the models are the most accurate ones available at present. Furthermore, since we analyse both the Mössbauer and localized-mode data with the same phonon models using the same Einstein-picture for the impurity, the interpretations of different experiments have been brought onto the same footing. The derived Einstein force-constant ratios should thus permit a sound qualitative discussion, and they are rigorously defined by Eqs. (22) and (25). Table 9 gives the localized mode frequencies from the mass-defect model, and where available the experimental frequencies are given in terms of force-constant ratios [Eq. (25)].

Prior to discussing the results, it is of interest to consider the experimental conditions under which the localized mode frequencies are deduced. The presence of free carriers in the samples poses a serious problem in semiconductors when one attempts to measure vibrational-mode absorption associated with donor or acceptor impurities because the absorption cross-section for free carriers can be as much as 10^3 times larger than the local-mode absorption cross-section[89]. It is therefore important that the carrier concentration and thus the carrier absorption is reduced without reduction in the localized-mode absorption.

A lowering of the temperature so that all free carriers are frozen out is no solution because the photo-ionization absorption is comparable to that of the free carriers. Electrical compensation appears the only feasible way. One method is double doping during the growth of the semiconductor. Here it is important that the compensating element does not introduce its own localized mode in the region of interest. This method usually yields at most one order of magnitude compensation of the free carriers and is therefore not used very frequently.

Another method for electrical compensation involves diffusion under conditions where the solubility of the diffusant (normally Li or Cu) is controlled by the impurity to be compensated. This technique has been applied for Si and GaAs, both of which have band gaps ≥ 1 eV. On the other hand, InSb and InAs with much smaller gaps are very unlikely candidates for diffusional compensation[90].

The most frequently used method is electrical compensation by means of light particle irradiation (e^-, p^+). The radiation damage thus introduced acts as trapping centres for the free carriers. However, the irradiation-induced defects may introduce new spectral features in the localized mode regime. This very serious problem has not been studied in great detail.

In the case of an isoelectronic substitution with group III or group V impurities in III-V semiconductors the defect will not contribute free carriers and hence electrical compensation is no problem. However, in some cases the introduction of group III or group V impurities leads to unexpected electrical activity, which in the literature is taken as evidence for a group III atom occupying a V-site or vice versa. The localized mode frequencies are considered under this assumption. However, no independent check as to the reliability of this assumption is made. When an impurity from columns II, IV or VI is introduced, the impurity is in general electrically active, and a reduction of the carrier concentration is needed. Thus it

appears that the assignment of localized mode frequencies to a given impurity configuration is somewhat problematic, at least if no independent tests are performed. Nevertheless we shall use the assignments given in the literature, keeping in mind, however, that force-constant ratios derived from infrared studies might have to be considered with some caution. In Mössbauer experiments, on the other hand, the lattice location of the impurity is unequivocally pinpointed by the isomer-shift measurement; however, the accuracy of the measured Debye temperatures is generally lower than for the localized-mode data.

4.4 Comparison of models and experimental data

The Mössbauer and localized-mode data are given in Tables 8 and 9, respectively, together with the deduced Einstein force-constant ratios. The Mössbauer and neutron diffraction data are seen to have sizeable errors that are reflected in the ϕ'/ϕ ratios. Nevertheless they represent a complete and systematic set of data for the six III-V semiconductors.

The impurity model of Mannheim [Eq. (23)] was also used to derive force-constant ratios (Table 8). Until recently it was assumed that this model should give quantitatively more realistic results compared to the Einstein–Debye model for semiconductors[4] as was concluded previously for metal hosts[44]. However, the validity of Mannheim's model for the zinc-blende lattice is doubtful since the model can only stabilize the fcc lattice[73]. For ^{119}Sn in group IV semiconductors it was found that the model overestimates the force-constant changes compared to a more realistic model[6], and that incidentally force-constant changes from the Einstein–Debye model seem relatively more realistic. The force-constant changes for the III-V compounds derived using Mannheim's model (Table 8) are again so large that no simple interpretation seems to emerge. Therefore no detailed discussion of these results will be given. It is concluded that the only applicable impurity model at present is the empirical Einstein–Debye model [Eq. (22)], which could be hoped to agree qualitatively with future more sophisticated treatments, as was found for Sn in group IV semiconductors.

The Einstein-Debye ratios ϕ'/ϕ (impurity force constant/host force constant) for the group IV impurities Sn and Si in the III-V compounds given in Tables 8 and 9 are displayed in Fig. 5. A trend is evident from the figure: the (ϕ'/ϕ) values for Sn in the In compounds are clearly smaller on the V sites than on the III sites, whereas in the Ga compounds the opposite trend is seen. The ϕ'/ϕ ratio is essentially determined by the Debye temperature ratio $\theta_D'(-2)/\theta_D(-2)$, as is seen from Eqs. (21) and (22). For the Ga compounds the III and V site values of $\theta_D'(-2)$ are very close, indicating nearly equal "effective" Sn force constants. From neutron-diffraction it was found that the host $\theta_D(-2)$ was lower on V sites than on III sites (see Tables 2–4), and it is this trend that is reflected in Fig. 5. For the In compounds the host $\theta_D(-2)$ clearly showed the opposite trend (Tables 5–7). The impurity $\theta_D'(-2)$ was furthermore lower on V sites than on III sites in the In compounds. The difference in the behaviour of $\theta_D'(-2)$ and $\theta_D(-2)$ results in the clear trend in ϕ'/ϕ displayed by Fig. 5.

A possible explanation for the trend of the Sn force constants in the Ga compounds may be seen in the Sn impurity's response to the host lattice ionicity. Isomer-shift measurements[91] demonstrated that substitutional Sn atoms probe the ionicity of the host, but due to its own intermediate electronegativity it only reflects partially the electronegativity of the replaced host atom. Likewise it is found that the Sn Debye temperatures are only little affected by the ionicity, since the effective force constants are almost equal on both lattice sites. However, the trend for Sn in the In compounds, on the other hand, remains unexplained at present. It is probably necessary to investigate the Sn-host system's electronic structure in more detail to resolve this problem.

The localized mode data for the four examples of substitutional Si impurities (Fig. 5 and Table 9) agree with these observations. GaAs:Si has a ratio ϕ'/ϕ greater than GaAs:Si. Furthermore the values of ϕ'/ϕ for GaP:Si and GaAs:Si are comparable with those of GaP:Sn and GaAs:Sn. It is also seen that the InP:Si and InP:Sn points are quite close. The experimental data for C impurities (Table 9) seem to agree reasonably well with these data.

Turning to the localized mode data for the isovalent B, Al, Ga, P, and As impurities (Table 9), no clear trends are seen, possibly owing to the fact that less complete systematic data are available. Since all the data

are within 7% of $\phi'/\phi = 1$, except for GaP:B, the mass-defect model is a rather good approximation for most isovalent impurities.

The amount of change in the impurity-host force constants and the sign of these changes are apparently not correlated with either the mass difference between the host and impurity atoms, or with interatomic distances and ionicity. The "simple rules" deduced from localized mode data[75] do not seem to account for the present results. Generally, the force-constant changes for the impurities as estimated here by the Einstein model tend to be lower than from previous evaluations of ^{119}Sn Mössbauer data in InP (based on X-ray-diffraction Debye temperatures)[85] or localized-mode data (by a RIM)[68].

5. CONCLUSION

The neutron- and X-ray diffraction data for perfect III-V semiconductors, which previously appeared inconsistent and controversial, have been examined critically by the present systematic study. Since the very accurate neutron data of Tibballs et al.[11] agree with our results, we conclude that reliable measurements of the thermal mean-square vibrational amplitudes of both atomic species have now been achieved (at 295 K) with an accuracy of a few per cent for all six III-V compounds. Correlations of the average mean-square amplitudes with the lattice constants and the ionicity of the III-V compounds could be understood qualitatively, whereas the differences in the amplitudes on the III and V sites (and a possible switchover of the relative amplitudes between Ga and In compounds) remain unexplained.

Phonon-density-of-states calculations were performed with most of the sophisticated models existing today. The models were compared with each other and tested against the neutron-diffraction data as well as with an analysis of the available specific-heat data. In all cases it was found that the present versions of the DDM and the RIM were insufficient, as were several SM fits. For GaP, GaAs, GaSb, and InSb accurate SMs exist, whereas the SMs for InP and InAs need reconsideration. It would also be of great value to measure the phonon dispersion in InAs by inelastic neutron scattering.

For impurity vibrations only a limited number of theoretical models are available. We have argued that a complete systematic fit of a reliable model, e.g. the shell model, to all the III-V compounds is a necessary prerequisite for constructing more realistic impurity models. Until this is achieved we suggest interpreting impurity data by means of the well-known mass-defect model, applying an Einstein-model picture to describe force-constant changes away from the idealized mass-defect case. The analytic Mannheim model applied in earlier analyses does not seem to give reliable quantitative results for the semiconductors.

Mössbauer data for ^{119}Sn occupying substitutional positions in all six III-V compounds have been obtained by a site-selective implantation technique. The measurements yielded the 12 impurity Debye temperatures, which could be directly related to model calculations. Localized-mode frequencies for light impurities reported in the literature were analysed with a simple impurity model.

The results were presented in terms of Einstein force-constant ratios ϕ'/ϕ, which are defined rigorously in the text. A trend for ^{119}Sn on the different lattice sites was noted: ϕ'/ϕ in the In compounds was significantly larger on the III sites than on the V sites, whereas the opposite was found in the Ga compounds. This trend was supported by the rather scarce localized mode data for Si and C impurities.

For the Ga compounds this trend can possibly be understood in terms of the Sn impurity's intermediate electronegativity relative to the host constituents. The ionicity of the host appears to be only partially reflected in the impurity Debye temperature or "effective" force constant. This picture does not seem to account for the behaviour of Sn in the In compounds, however. Also, previously suggested "simple rules" for force-constant changes of donors and acceptors in the III-V semiconductors appear doubtful in view of the present results.

APPENDIX

MANNHEIM MODEL FOR ZINC-BLENDE LATTICES[92]

The Mannheim model for a substitutional impurity using only nearest-neighbour central forces was derived by Petersen et al.[4] for the diamond lattice. Here we derive the $\theta_D'(-2)$ formula [Eq. (26) of Ref. 4] for the zinc-blende structure.

With the definitions of Ref. 4 we may write

$$[1 - \varepsilon + (\lambda - \varepsilon)S]U_1 - 1/4\lambda S(U_2 + U_3) = G_1 \tag{A1}$$

$$-4(\varepsilon M_1 - \lambda M_4)\omega^2(G_2 + 2G_3)U_1 + \left[1 - \lambda M_4\omega^2(G_2 + 2G_3)\right](U_2 + U_3) = 4G_2 + 8G_3 \quad , \tag{A2}$$

where $M_1 = M_{(000)}$ and $M_4 = M_{(111)}$. These equations generalize Eqs. (39) and(40) of Ref. 4 to the zinc-blende structure. Since $M_4 \neq M_1$ in zinc blende, the solution of Eqs. (A1) and (A2) is a complicated expression, and we therefore only give the result for $\omega = 0$:

$$(1 - \lambda)U_1 + 1/4\lambda(U_2 + U_3) = G_1 \, , \tag{A3}$$

which yields

$$U_2 + U_3 = 4G_2 + 8G_3 \quad . \tag{A4}$$

This can be rewritten in terms of Debye temperatures[6]:

$$u_1(\omega=0) = G_1(\omega=0) - \frac{1}{\phi_{xx}(000, 000)}\left(\frac{\phi_{xx}(000, 000)}{\phi'_{xx}(000, 000)} - 1\right) \tag{A5}$$

$$\theta'_D(-2) = \theta_D(-2)\sqrt{\frac{M_1}{M'_1}}\left[1 + \frac{5}{9}\left(\frac{\theta_D(-2)}{\theta_D(+2)}\right)^2\left(\frac{\phi_{xx}(000, 000)}{\phi'_{xx}(000, 000)} - 1\right)\right]^{-1/2} \quad . \tag{A6}$$

Here $\theta_D(n)$ refer to the site (000), and $\theta'_D(-2)$ is the impurity Debye temperature.

The condition for the occurrence of a localized mode is that the determinant of the real part of the system of Eqs. (A1) and (A2) should be zero, and $g(\omega) \equiv 0$. The resulting expression is not simple, and it may be pointed out that the condition in all cases must be evaluated numerically.

Acknowledgements

It is a pleasure to acknowledge the excellent experimental conditions at the Risø National Laboratory and at the ISOLDE facility at CERN, where most of the experiments have been performed. Discussions with E. Antoncik were of great value to us. We are grateful to the cyclotron staff of the Niels Bohr Institute for the α-irradiations, and to H.L. Nielsen for the radiochemical separation of ^{119}Sb from ^{119m}Te. We would like to thank J.E. Tibballs for sending us neutron-diffraction results prior to publication, and MCP Electronics Ltd. for supplying samples for the neutron-diffraction experiments. This work has been supported in part by the Danish Natural Science Research Council and by the Danish Accelerator Physics Council.

REFERENCES AND FOOTNOTES

1) B. Welch, F.H. Eisen and J.S. Higgins, J. Appl. Phys. **45**, 3685 (1974).
2) G. Weyer, A. Nylandsted-Larsen, B.I. Deutch, J.U. Andersen and E. Antoncik, Hyperfine Interactions 1, 93 (1975).
3) E. Antoncik, Hyperfine Interactions **1**, 329 (1976).
4) J.W. Petersen, O.H. Nielsen, G. Weyer, E. Antoncik and S. Damgaard, Phys. Rev. **B21**, 4292 (1980) and 22, 3135E (1980).
5) V.I. Goldanskii and R.H. Herber, Chemical applications of Mössbauer spectroscopy (Academic Press, New York, 1968).
6) O.H. Nielsen, "Lattice dynamics of substitutional ^{119m}Sn in silicon, germanium and α-tin using an adiabatic bond charge model", to be published in Phys. Rev. B.
7) P.D. Mannheim, Phys. Rev. **165**, 1011 (1968); P.D. Mannheim and A. Simopoulos, Phys. Rev. **165**, 845 (1968); P.D. Mannheim and S.S. Cohen, Phys. Rev. **B4**, 3748 (1971); P.D. Mannheim, Phys. Rev. **B5**, 745 (1972).
8) H. Bilz and W. Kress, "Phonon dispersion relations in insulators", Springer series in solid state sciences (Springer, Berlin, 1979), Vol. 10.
9) W. Weber, Phys. Rev. Lett. **33**, 371 (1974); Phys. Rev. **B15**, 4789 (1977).
10) G. Weyer, J.W. Petersen, S. Damgaard, H.L. Nielsen and J. Heinemeier, Phys. Rev. Lett. **44**, 155 (1980).
11) J.E. Tibballs, S.M. Feteris and Z. Barnea, "Neutron diffraction determination of mean-square atomic displacements in InAs and GaSb", to appear in Australian J. Phys.
12) B. Moss, R.K. McMullan and Koetzle, J. Chem. Phys. **73**, 495 (1980).
13) G.J.McIntyre, G.R. Moss and Z. Barnea, Acta Crystallogr. **A36**, 482 (1980).
14) M.S. Lehmann and F.K. Larsen, Acta Crystallogr. **A30**, 580 (1974).
15) P. Coppens, *in* Crystallographic computing (ed. F.R. Ahmed) (Munksgaard, Copenhagen, 1970), p. 255.
16) M.J. Cooper *in* Thermal neutron diffraction (ed. B.T.M. Willis) (Univ. Press, Oxford, 1970).
17) M.J. Cooper, Acta Crystallogr. **A27**, 148 (1971).
18) M. Merisalo and J. Kurittu, J. Appl. Crystallogr. **11**, 179 (1978).
19) R. Weil and W.O. Groves, J. Appl. Phys. **39**, 4049 (1968).
20) C.W. Garland and K.C. Park, J. Appl. Phys. **33**, 759 (1962).
21) J.T. Lin and Chuen Wong, J. Phys. Chem. Solids **33**, 241 (1972).
22) F.S. Hickernell and W.R. Gayton, J. Appl. Phys. **37**, 462 (1966).
23) Y.A. Burenkov, S.Y. Davydov and S.P. Nikanorov, Sov. Phys.–Solid State **17**, 1446 (1976).
24) L.J. Slutsky and C.W. Garland, Phys. Rev. **113**, 167 (1959).
25) G.E. Bacon, *in* the Neutron diffraction newsletter, February 1977 (ed. W.B. Yelon) (University of Missouri Research Reactor Facility, Columbia, Missouri).
26) J.P. Becker and F. Coppens, Acta Crystallogr. **A31**, 417 (1975).
27) V.T. Bublik and S.S. Gorelik, Krist. u. Tech. **12**, 859 (1977).
28) M.G. Shumskii, V.T. Bublik, S.S. Gorelik and M.A. Gorevich, Sov. Phys.–Crystallogr. **16**, 674 (1972) [transl. of Kristallografiya **16**, 779 (1971)].
29) G. Pepe, P. Masri, M. Bienfait and L. Dobrzynski, Acta Crystallogr. **A30**, 290 (1974).
30) K.S. Liang, C.S. Goenzer and A.I. Bienenstock, Bull. Am. Phys. Soc. **15**, 1637 (1970).
31) N.N. Sirota, Acta Crystallogr. **A25**, 223 (1969).
32) H.-G. Brühl, Krist. u. Tech. **15**, K83 (1980).
33) R. Uno, P. Ukano and K. Yukino, J. Phys. Soc. Japan **28**, 437 (1970).
34) G. Arnold and N. Nereson, Phys. Rev. **131**, 2098 (1963).
35) D.H. Bilderback and R. Colella, Phys. Rev. **B13**, 2479 (1976).
36) R.N. Kyutt, Sov. Phys.–Crystallogr. **19**, 705 (1975) [transl. of Kristallografiya **19**, 1133 (1974)].

37) M.T. Yin and M.L. Cohen, Phys. Rev. Lett. **45**, 1004 (1980).
38) O.H. Nielsen and W. Weber, J. Phys. **C 13**, 2449 (1980).
39) R. Colella, Phys. Rev. **B 3**, 4308 (1971).
40) J.P. Walter and M.L. Cohen, Phys. Rev. **B 4**, 1877 (1981).
41) T.P. Humphries and G.P. Srivastava, Phys. Status Solidii **(b) 103**, K85 (1981).
42) M.J. Cooper, K.D. Rouse and H. Fuess, Acta Crystallogr. **A 29**, 49 (1973).
43) A.A. Maradudin, E.W. Montroll, G.H. Weiss and I.P. Ipatova, Theory of lattice dynamics in the harmonic approximation, 2nd ed. (Academic Press, New York, 1971).
44) J.M. Grow, D.G. Howard, R.H. Nussbaum and M. Takeo, Phys. Rev. **B 17**, 15 (1978).
45) $n = 0, -3$ are special cases:

$$\theta_D(0) = (\hbar/k_B) \exp\left(\frac{1}{3} + \int_0^\infty \ln(\omega) g(\omega)\, d\omega\right) \text{ and } \theta_D(-3) = (\hbar/k_B)(A/3)^{-1/3},$$

where $g(\omega) = A\omega^2$ near $\omega = 0$. If the Debye model density of states is used with Eq. (12) it becomes $\theta_D(n) = \theta_D$ for all n.
46) T.H.K. Barron, W.T. Berg and J.A. Morrison, Proc. Roy. Soc. London **A 242**, 478 (1957).
47) S.K. Sinha, Crit. Rev. Solid State Sci. **2**, 1 (1971).
48) W. Cochran, Crit. Rev. Solid State Sci. **4**, 273 (1973).
49) S.S. Jaswal, *in* Proc. Int. Conf. on Lattice Dynamics, 1977 (Flammarion, Paris, 1978), p.41; J. Phys. **C 11**, 3559 (1978).
50) K. Kunc, M. Balkanski and M.A. Nusimovici, Phys. Rev. **B 104346** (1975); Phys. Status Solidi **(b) 71** 341 (1975); **72**, 229 (1975), and **72**, 249 (1975).
51) P.H. Borcherds and K. Kunc, J. Phys. **C 11**, 4145 (1978).
52) P.H. Borcherds, K. Kunc, G.F. Alfrey and R.L. Hall, J. Phys. **C 12**, 4699 (1979).
53) J.F. Vetelino, S.P. Guar and S.S. Mitra, Phys. Rev. **B 5**, 2360 (1972).
54) D.N. Talwar and B.K. Agrawal, Solid State Commun. **14**, 25 (1974); J. Phys. **C 7**, 2981 (1974).See also M.S. Kushwaha, Phys. Rev. **B 24**, 2115 (1981).
55) J.S. Reid, "Debye–Waller factors of zinc-blende structure compounds", to be published in Acta Crystallogr. A.
56) K. Kunc and O.H. Nielsen, Comput. Phys. Commun. **16**, 181 (1979) and **17**, 413 (1979).
57) O.H. Nielsen and S.S. Jaswal, to be published in Comput. Phys. Commun.
58) G. Gilat, Methods in Comput. Phys. **15**, 317 (1976).
59) A.H. MacDonald, S.H. Vosko and P.T. Coleridge, J. Phys. **C 12**, 2991 (1979).
60) K. Kunc and H. Bilz, Solid State Commun. **19**, 1027 (1976).
61) J.L. Yarnell, J.L. Warren, R.G. Wenzel and P.J. Dean, *in* Neutron inelastic scattering (IAEA, Vienna, 1968), Vol. 1, p. 301.
62) V.V. Tarassov and A.F. Demidenko, Phys. Status Solidi **30**, 147 (1968).
63) J.C. Irwin and J. La Combe, J. Appl. Phys. **45**, 567 (1974).
64) G. Dolling and J.L.T. Waugh, *in* Lattice dynamics (ed. R.F. Wallis) (Pergamon Press, London, 1965), p. 19.
65) U. Piesbergen, Z. Naturforsch. **18 A**, 141 (1963).
66) T.C. Cetas, C.R. Tilford and C.A. Swenson, Phys. Rev. **174**, 835 (1968).
67) M.K. Farr, J.G. Traylor and S.K. Sinha, Phys. Rev. **B 11**, 1587 (1975).
68) M. Vandevyver and P. Plumelle, J. Phys. Chem. Solids **38**, 765 (1977).
69) D.L. Price, J.M. Rowe and R.M. Nicklow, Phys. Rev. **B 3**, 1268 (1971).
70) J.C. Holste, Phys. Rev. **B 6**, 2495 (1972).
71) K. Kunc, private communication.
72) H.J. Lipkin, Ann. Phys. **26**, 115 (1964).
73) P.H. Dederichs and R. Zeller, Springer tracts in modern physics (Springer, Berlin, 1980), Vol. 87.
74) P.G. Dawber and R.J. Elliott, Proc. Roy. Soc. London, Ser. **A 273**, 222 (1963); Proc. Phys. Soc. London **81**, 453 (1963).

75) M. Vandevyver, D.N. Talwar, P. Plumelle, K. Kunc and M. Zigone, Phys. Status Solidii (b)99, 727 (1980); M. Vandevyver and D.N. Talwar, Phys. Rev. **B 21**, 3405 (1980).
76) J.B. Page, Jr. and B.G. Dick, Phys. Rev. **163**, 910 (1967); J.B. Page, Jr. and D. Strauch, Localized excitations in solids (Plenum Press, N.Y., 1968), p. 559; J.B. Page, Jr. and D. Strauch, Phys. Status Solidii **24**, 469 (1967); D. Strauch, Phys. Status Solidii **30**, 495 (1968).
77) J.W. Petersen, S. Damgaard, J. Heinemeier and G. Weyer, *in* Proc. EPS Conf. on Nuclear Physics Methods in Materials Research (eds. K. Bethge, H. Baumann, H. Jex and F. Ranch) (Vieweg, Braunschweig, 1980), p. 448.
78) N.E. Holm and G. Weyer, J. Phys. **C 13**, 1109 (1980).
79) G. Weyer, A. Nylandsted-Larsen, N.E. Holm and H.L. Nielsen, Phys. Rev. **B 21**, 4939 (1980).
80) H. Ravn, L.C. Carraz, J. Denimal, E. Kugler, M. Skareslad, S. Sundell and L. Westgaard, Nucl. Instrum. Methods **139**, 267 (1976).
81) H. Ravn, Phys. Rep. **54**, 201 (1979).
82) G. Weyer, Mössbauer effect methodology (eds. I.J. Gruverman and C.W. Seide)(Plenum Press, New York and London, 1976), Vol. 10, p. 301; Nucl. Instrum Methods **186**, 201 (1981).
83) G. Weyer, S. Damgaard, J.W. Petersen and J. Heinemeier, Phys. Status Solidii (b)**98**, K147 (1980).
84) G. Weyer, S. Damgaard, J.W. Petersen and J. Heinemeier, J. Phys. **C 13**, L181 (1980).
85) S. Damgaard, J.W. Petersen and G. Weyer, J. Phys. **C 14**, 993 (1981).
86) A.S. Barker, Jr. and A.J. Sievers, Rev. Mod. Phys. **47**, Suppl. 2 (1975).
87) M.R. Brozel, R.C. Newman and M.G. Astles, J. Phys. **C 11**, L377 (1978).
88) E. Jahne, P. Kleinert, B.Kh. Bairamov and V.V. Toporov, Phys. Status Solidii (b) **104**, 531 (1981).
89) T.S. Moss, Optical properties of semiconductors (Butterworth, London, 1951).
90) W.G. Spitzer, *in* Festkörperprobleme XI (ed. O. Madelung)(Pergamon Press, London, 1971), p. 1.
91) J.W. Petersen, S. Damgaard and G. Weyer, to be published.
92) This appendix corrects the erratum of Ref. 4.

Table I

Mean-square vibrational amplitudes in III-V semiconductors determined by neutron or X-ray diffraction. The values are one-dimensional amplitudes in Å^2.

	$\langle u^2\rangle_{III}$	$\langle u^2\rangle_{V}$	Source, comment		$\langle u^2\rangle_{III}$	$\langle u^2\rangle_{V}$	Source, comment
GaP	0.0092(5)	0.0095(5)	this work, neutrons	InP	0.0116(6)	0.0099(5)	this work, neutrons
	0.0067	0.0100	Refs. 27, 28, X-ray, single crystal, 6 reflections		0.0098	0.0137	Refs. 27, 28, X-ray, single crystal, 6 reflections
	0.0045(1)	0.0059(3)	Ref. 29, X-ray, single crystal, no TDS correction, no extinction observed		0.0164	0.0190	Ref. 31, X-ray, powder
	0.0056 0.0115 0.0065(3)	0.0038 0.0113 0.0076(3)	Ref. 30, X-ray, powder Ref. 31, X-ray, powder Ref. 32, X-ray, powder				
GaAs	0.0082(8) 0.0077	0.0104(8) 0.0063	this work, neutrons Refs. 27, 28, X-ray, single crystal, 6 reflections	InAs	0.0123(5) 0.0116(2)	0.0098(4) 0.0107(1)	this work, neutrons Ref. 11, neutrons, single crystal, TDS correction anisotropic extinction correction
	0.0116	0.0117	Ref. 33, X-ray, powder, TDS correction		0.0127	0.0107	Refs. 27, 28, X-ray, single crystal, 6 reflections
	0.0025	0.0071	Ref. 31, X-ray, powder, TDS correction		0.0127	0.0127	Ref. 31, X-ray, powder
	0.0100	0.0100	Ref. 34, neutrons, powder		0.0079	0.0078	Ref. 34, neutrons, powder
GaSb	0.0107(5)	0.0113(5)	this work, neutrons	InSb	0.0161(6) 0.0201(9) 0.0251(11)	0.0140(6) 0.0188(9) 0.0227(6)	this work, neutrons, 295 K this work, neutrons, 373 K this work, neutrons, 473 K
	0.0121(1)	0.0107(1)	Ref. 11, neutrons, single crystal, TDS correction, anisotropic extinction correction		0.0170	0.0142	Ref. 35, X-ray, single crystal, 9 reflections (temperature) $\theta_{In} = 148.5$ K, $\theta_{Sb} = 157.5$ K
	0.0123	0.0098	Refs. 27, 28, X-ray, single crystal, 6 reflections		0.0189(13)	0.0155(9)	Ref. 36, X-ray, single crystal, 4 reflections (temperature)
	0.0108	0.0091	Ref. 31, X-ray, powder, TDS correction		0.0125	0.0108	Refs. 27, 28, X-ray, single crystal, 6 reflections
	0.0081	0.0081	Ref. 34, neutrons, powder		0.0119	0.0119	Ref. 34, neutrons, powder

Table 2

Weighted moments of GaP density-of-states functions [cf. Eq. (12)] expressed as Debye temperatures in K. Source of model or experiment is indicated.

−3	−2.5	−2	−1	0	1	2	3	4	5	6	Reference
Ga atom											
396	311	288	281	295	321	352	383	411	434	453	DDM, Ref. 50
380	313	292	284	294	317	347	377	405	428	447	SM, Ref. 60
390	330	314	319	347	387	425	457	480	498	510	SM, Ref. 61
398	313	289	278	288	309	338	370	400	425	445	SM, Ref. 52
413	361	352	376	423	467	499	520	534	543	549	RIM, Ref. 50
		262(7)									Neutrons
P atom											
529	521	542	603	646	656	655	651	646	642	638	DDM
506	516	543	606	626	639	638	633	627	621	616	SM
508	432	426	470	528	569	589	597	600	600	599	SM
531	536	563	620	664	663	656	649	641	635	629	SM
532	380	358	379	436	496	537	560	573	579	583	RIM
		392(10)									Neutrons
Average											
444	373	360	383	437	488	526	550	565	574	580	DDM
425	373	364	387	429	478	513	536	549	557	561	SM
434	369	357	380	428	478	514	536	550	558	563	SM
446	377	364	384	437	486	522	545	559	567	571	SM
458	370	355	378	429	481	519	541	554	562	567	RIM
		307(9)									Neutrons
			376	430	478	511(1)		542(2)		557(11)	cv, Refs. 62, 63

Table 3

Weighted moments of GaAs density-of-states functions [cf. Eq. (12)] expressed as Debye temperatures in K. Source of model or experiment is indicated.

−3	−2.5	−2	−1	0	1	2	3	4	5	6	Reference
Ga atom											
339	315	316	350	395	421	434	439	441	441	440	DDM, Ref. 50
307	266	255	264	291	320	344	360	371	378	382	SM, Ref. 60
343	274	259	268	296	327	352	368	379	385	390	SM (Bi), Ref. 64
350	304	297	318	353	381	397	406	410	412	413	SM (Bii),Ref. 64
338	277	265	279	315	349	372	386	394	399	401	SM (Ci), Ref. 64
339	289	280	297	333	362	381	392	399	402	405	SM (Cii),Ref. 64
355	350	359	394	415	428	433	433	432	430	429	RIM, Ref. 50
		278(14)									Neutrons
As atom											
324	262	247	252	279	310	337	357	370	380	386	DDM
305	295	299	328	361	384	397	403	406	407	408	SM
340	294	286	304	338	366	385	395	401	405	407	SM (Bi)
337	268	252	258	285	316	341	359	371	379	385	SM (Bii)
334	285	276	292	327	357	377	389	396	400	403	SM (Ci)
327	271	260	274	310	344	367	382	390	396	399	SM (Cii)
338	248	229	228	247	277	306	329	344	356	364	RIM
		237(10)									Neutrons
Average											
331	284	275	293	332	366	388	402	410	415	418	DDM
306	279	275	292	324	352	372	383	390	394	396	SM
342	284	272	285	316	347	369	382	390	396	399	SM (Bi)
343	284	272	285	317	348	370	384	392	397	400	SM (Bii)
336	281	270	286	321	353	374	387	395	399	402	SM (Ci)
333	279	269	285	321	353	374	387	395	399	402	SM (Cii)
346	284	273	289	320	353	375	388	395	400	403	RIM
		255(12)									Neutrons
347(2)	294	285	298	326	351	370(1)		389(2)		397(7)	cv, Refs. 65, 66

Table 4

Weighted moments of GaSb density-of-states functions [cf. Eq. (12)] expressed as Debye temperatures in K. Source of model or experiment is indicated.

−3	−2.5	−2	−1	0	1	2	3	4	5	6	Reference
Ga atom											
239	215	212	234	272	304	322	332	337	340	341	SM, Ref. 67
277	236	232	255	293	320	335	342	345	345	345	SM, Ref. 60
295	210	196	205	232	268	296	314	324	329	333	RIM, Ref. 68
		227(1)									Neutrons, Ref. 11
		242(6)									Neutrons
Sb atom											
202	193	194	213	244	273	293	306	314	319	322	SM
232	197	189	196	220	247	270	286	297	305	311	SM
250	226	223	246	274	301	318	328	334	337	340	RIM
		183(1)									Neutrons, Ref. 11
		178(5)									Neutrons
Average											
218	203	203	223	258	288	308	319	326	330	332	SM
250	214	207	222	254	284	304	316	324	328	330	SM
269	217	208	224	252	284	308	321	329	333	336	RIM
		201(1)									Neutrons, Ref. 11
		202(6)									Neutrons
270(2)	223	216	229	255	278	298(1)		315(1)		322(6)	cv, Refs. 65, 66

Table 5

Weighted moments of InP density-of-states functions [cf. Eq. (12)] expressed as Debye temperatures in K. Source of model or experiment is indicated.

−3	−2.5	−2	−1	0	1	2	3	4	5	6	Reference
In atom											
233	197	184	179	189	210	239	273	305	332	354	SM, Ref. 51
219	178	164	161	175	202	237	273	305	332	354	RIM, Ref. 68
		181(5)									Neutrons
P atom											
375	408	450	540	564	573	570	563	556	550	544	SM
353	400	456	565	606	606	598	589	581	574	569	RIM
		383(10)									Neutrons
Average											
274	245	241	269	327	391	437	463	478	486	491	SM
257	223	219	251	326	404	455	482	498	506	512	RIM
		231(8)									Neutrons
	243	242	278	339	398	438(1)		473(2)		488(12)	cv, Ref. 65

Table 6

Weighted moments of InAs density-of-states functions [cf. Eq. (12)] expressed as Debye temperatures in K. Source of model or experiment is indicated.

−3	−2.5	−2	−1	0	1	2	3	4	5	6	Reference
In atom											
233	188	178	180	201	226	249	269	283	293	301	SM, (a) of Ref. 51
224	190	180	183	194	216	239	258	272	282	290	SM, (b) of Ref. 51
		181(2)									Neutrons, Ref. 11
		176(4)									Neutrons
As atom											
262	259	269	305	359	372	374	373	371	369	367	SM
263	262	272	313	321	343	353	356	356	355	354	SM
		233(1)									Neutrons, Ref. 11
		244(5)									Neutrons
Average											
240	214	210	227	269	299	318	329	336	340	342	SM
240	216	212	231	250	279	302	315	322	327	329	SM
		201(2)									Neutrons, Ref. 11
		201(5)									Neutrons
251(1)	209	204	222	256	289	312(1)		334(2)		343(8)	cv, Refs. 65, 66

Table 7

Weighted moments of InSb density-of-states functions [cf. Eq. (12)] expressed as Debye temperatures in K. Source of model or experiment is indicated.

−3	−2.5	−2	−1	0	1	2	3	4	5	6	Reference
In atom											
205	190	195	230	264	283	290	292	292	292	291	DDM, Ref. 50
185	152	146	157	180	208	230	244	252	257	260	SM, Ref. 51
193	155	149	161	190	219	240	252	259	263	266	SM, Ref. 69
184	183	190	230	262	283	291	293	293	292	291	RIM, Ref. 50
188	156	151	167	199	230	250	261	268	271	273	DIM, Ref. 49
		153(3)									Neutrons
Sb atom											
196	137	127	130	148	175	200	218	230	238	244	DDM
184	171	172	197	226	251	265	272	276	277	278	SM
191	162	158	175	208	236	254	263	269	271	273	SM
140	124	117	122	141	168	191	209	220	229	235	RIM
185	153	148	164	194	224	245	257	264	268	271	DIM
		160(4)									Neutrons
Average											
200	156	150	166	198	229	249	260	267	270	272	DDM
185	160	157	175	202	230	248	259	264	268	270	SM
192	158	153	168	199	228	247	258	264	268	270	SM
156	144	141	160	193	225	246	258	264	268	270	RIM
187	155	150	165	196	227	248	259	266	270	272	DIM
		156(4)									Neutrons
207(1)	168	163	176	203	228	247(1)		264(1)		271(6)	cv, Refs. 65, 66

Table 8

Results from ^{119}Sn Mössbauer spectroscopy. Lattice constant a, host masses, and neutron diffraction $\theta_D(-2)$ from Tables 2–7 are given. ^{119}Sn isomer shift (IS) and $\theta'_D(-2)$ on the different lattice sites are given. Mass-defect model [Eq. (20)] $\theta'_D(-2)$ (MD) values are used to deduce Einstein–Debye force-constant ratios ϕ'/ϕ (E–D) [cf. Eq. (22)]. ϕ'/ϕ (Mannheim) values [Eq. (23)] are also shown.

Host	a [Å]	Sn site	IS [mm/s]	Host mass	$\theta_D(-2)$ [K]	$\theta'_D(-2)$ M.D.	$\theta'_D(-2)$ Mössbauer	$(\phi'/\phi)_{ED}$	$(\phi'/\phi)_M$	Phonon model
GaP	5.45	Ga	1.58(3)	69.72	262(7)	201(5)	226(5)	1.26(4)	3.22	Ref.61
		P	1.85(5)	30.97	392(10)	200(5)	233(10)	1.36(7)	10.6	
GaAs	5.65	Ga	1.76(3)	69.72	278(10)	213(11)	202(5)	0.90(5)	0.73	Section c (ii) of Ref. 64
		As	1.83(4)	74.92	237(10)	181(8)	200(7)	1.22(7)	2.85	
GaSb	6.12	Ga	1.81(4)	69.72	227(1)	174(1)	177(4)	1.03(2)	1.14	Ref.60
		Sb	1.89(5)	121.75	183(1)	185(1)	187(10)	1.02(5)	1.08	
InP	5.87	In	1.61(3)	114.82	181(5)	178(5)	202(6)	1.29(5)	3.11	Ref.51
		P	1.92(3)	30.97	383(10)	195(5)	186(10)	0.91(7)	–	
InAs	6.04	In	1.77(4)	114.82	181(2)	178(2)	180(4)	1.02(3)	1.06	Section a of Ref. 51
		As	1.91(3)	74.92	233(1)	178(1)	165(10)	0.86(5)	–	
InSb	6.48	In	1.98(3)	114.82	153(3)	150(3)	165(4)	1.21(4)	5.28	Ref.69
		Sb	1.94(5)	121.75	160(4)	162(4)	157(5)	0.94(4)	0.77	

Table 9

Localized mode results. Mass-defect model frequencies [Eq. (24)] are given in cm^{-1}, using the indicated phonon model. Available experimental frequencies are shown below expressed as an Einstein force-constant [Eq. (25)].

Host	Site	^{10}B	^{11}B	^{12}C	^{13}C	^{14}C	^{27}Al	^{28}Si	^{30}Si	^{31}P	Ga	^{75}As	Phonon model
GaP	Ga	649 0.84	624 0.83	603	583	566	451 0.97	447 1.08	438 1.09	435	—	—	Ref.61
	P	585	561	540 1.26	521 1.25	505	399	—	—	—	—	—	
GaAs	Ga	558 0.94	534 0.94	513	494	478	361 1.01	356 1.16	346 1.17	341	—	—	Sect. c(ii) of Ref. 64
	As	560	536	515 1.28	497 1.27	481	364	358 1.24	349 1.24	345 1.06	—	—	
GaSb	Ga	487	466	447	431	417	310 1.05	305	297	292	—	—	Ref. 60
	Sb	523	500	481	463	448	337	333	323	319 1.03	245	241 0.99	
InP	In	487 1.25	470 1.24	456	443	433	366	364 1.40	360 1.37	358	—	—	Ref.51
	P	549	524	502	483	466	345	341	—	—	—	—	
InAs	In	462	443	426	411	398	305	301	294	290	235	—	Section b of Ref. 51
	As	537	513	491	473	456	335	329	319	314 0.93	—	—	
InSb	In	449	429	412	397	384	287 1.06	282	274	270	202 0.94	198	Ref. 69
	Sb	486	464	446	429	414	307	302	293	288 1.04	210	205 0.95	

Figure captions

Fig. 1 : Mean-square amplitudes at 295 K versus lattice constants or interatomic distances. The ○ denote cations and the Δ anions, and the ● and ▲ the corresponding data of Tibballs et al.[11]. The □ denote calculated values[38] for group IV semiconductors. For α-Sn the Mössbauer value[4], θ_D = 164(5) K, was used. The solid lines give the average trends for Ga and In compounds separately.

Fig. 2 : Mössbauer spectrum of ^{119}Sn in GaSb after implantation of ^{119}In, (a) before and (b) after an annealing of the sample for 1 min at 200 °C.

Fig. 3 : Mössbauer spectrum of ^{119}Sn in GaSb after implantation of ^{119}Sb at 325 °C.

Fig. 4 : Mössbauer–Debye temperatures $\theta'_D(-2)$ from Table 8 displayed against the lattice constant. The ○ denote Sn on a III site and the Δ denote Sn on a V site.

Fig. 5 : Einstein-model force-constant ratios ϕ'(impurity)/ϕ(host) from Tables 8 and 9 plotted versus the lattice constants of the III-V compounds. The ○ indicate Sn on a III site, the Δ Sn on a V site, the ● Si on a III site, and the ▲ Si on a V site. The respective trends for Sn on III and V sites for Ga and In compounds, are indicated by dashed and solid lines.

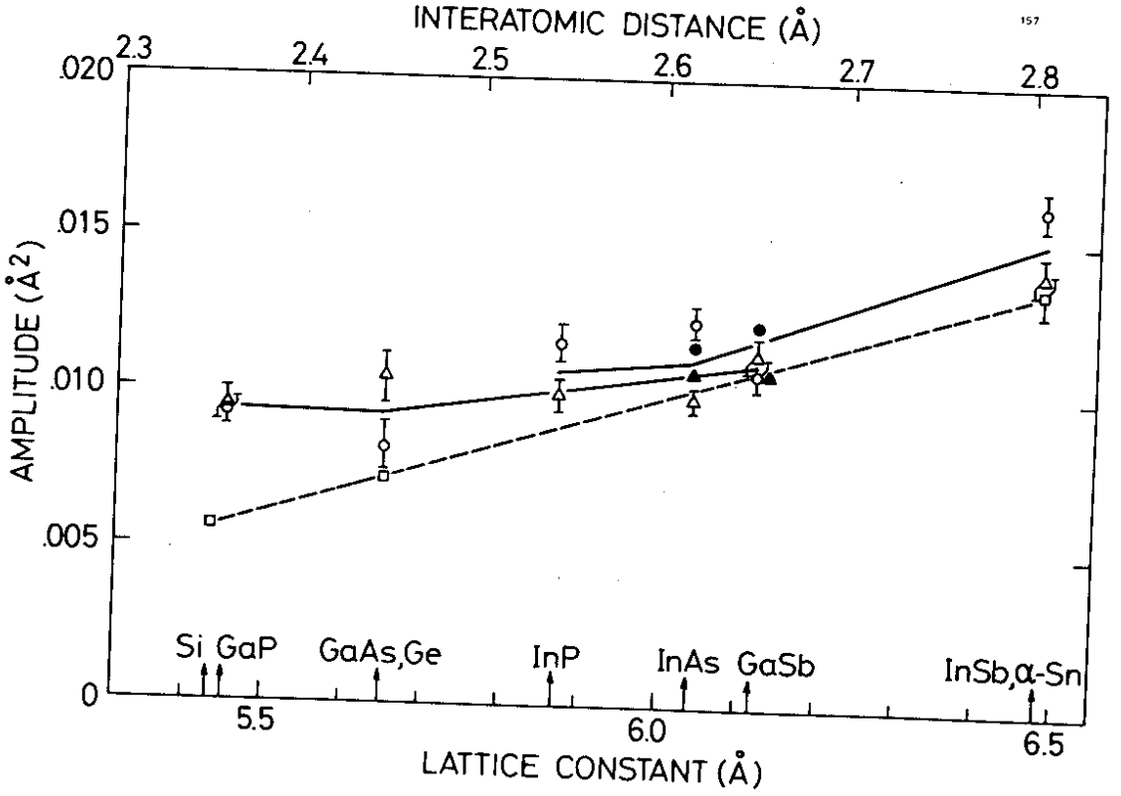
INTERATOMIC DISTANCE (Å)
2.3
2.4
2.5
2.6
2.7
2.8
.020
.015
.010
.005
0
AMPLITUDE (Å²)
Si GaP
GaAs,Ge
InP
InAs GaSb
InSb,α-Sn
5.5
6.0
6.5
LATTICE CONSTANT (Å)

Fig. 1

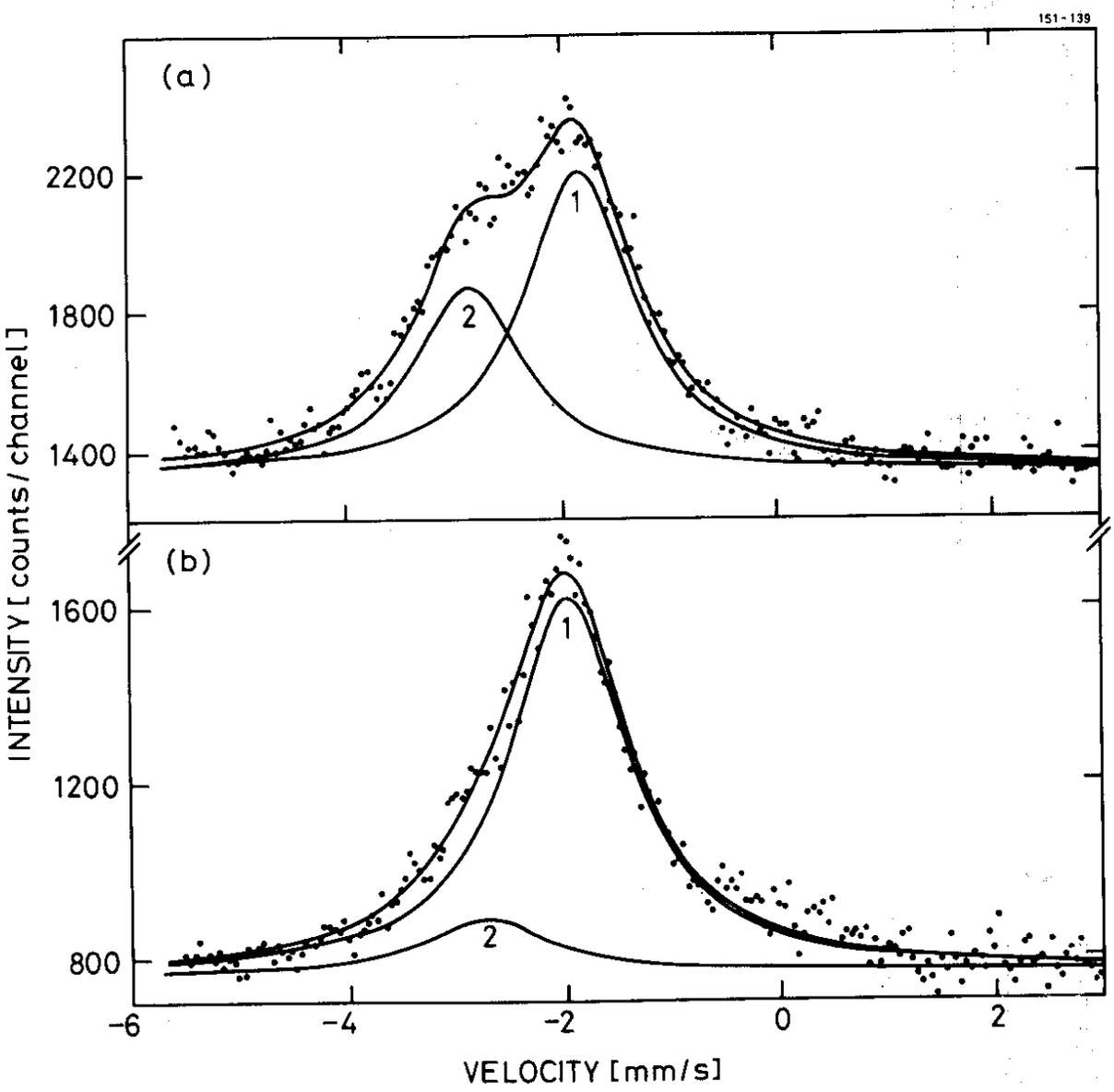
151-139
(a)
2200
1800
1400
1
2
(b)
1600
1200
800
1
2
INTENSITY [counts/channel]
-6
-4
-2
0
2
VELOCITY [mm/s]

Fig. 2

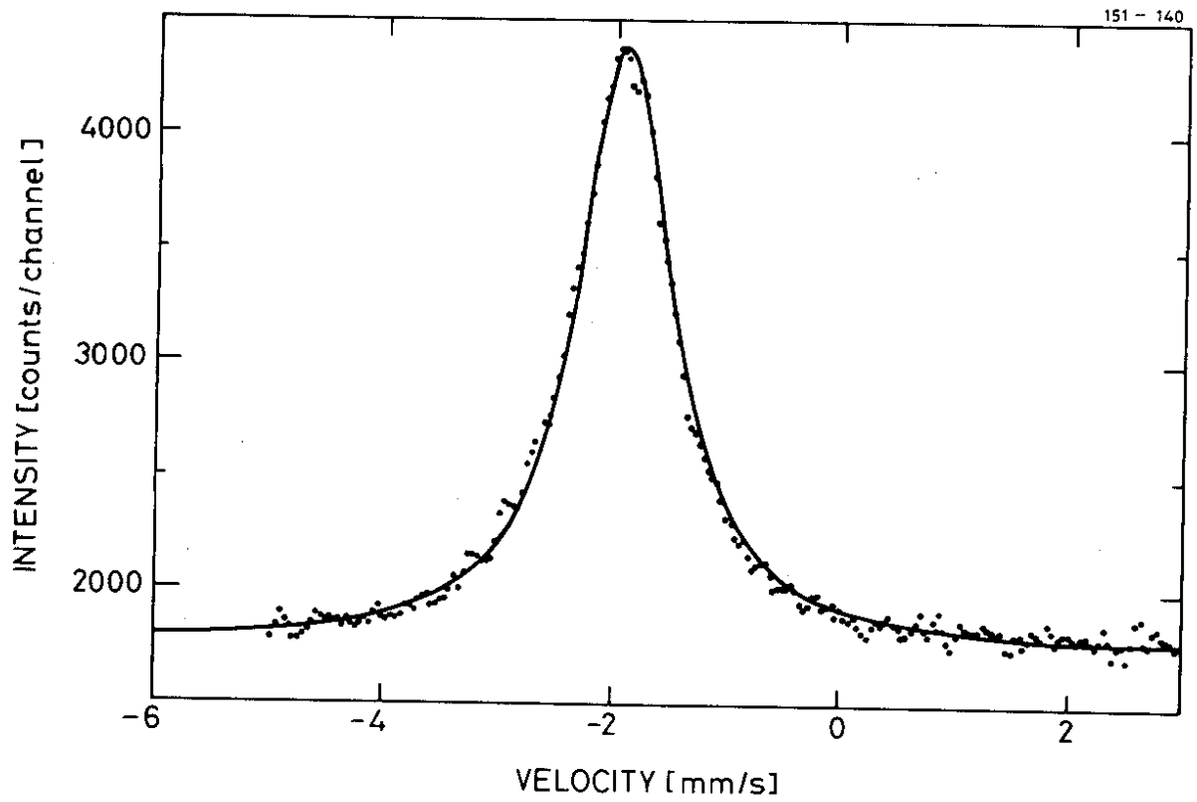
151 - 140
INTENSITY [counts/channel]
4000
3000
2000
-6
-4
-2
0
2
VELOCITY [mm/s]

Fig. 3

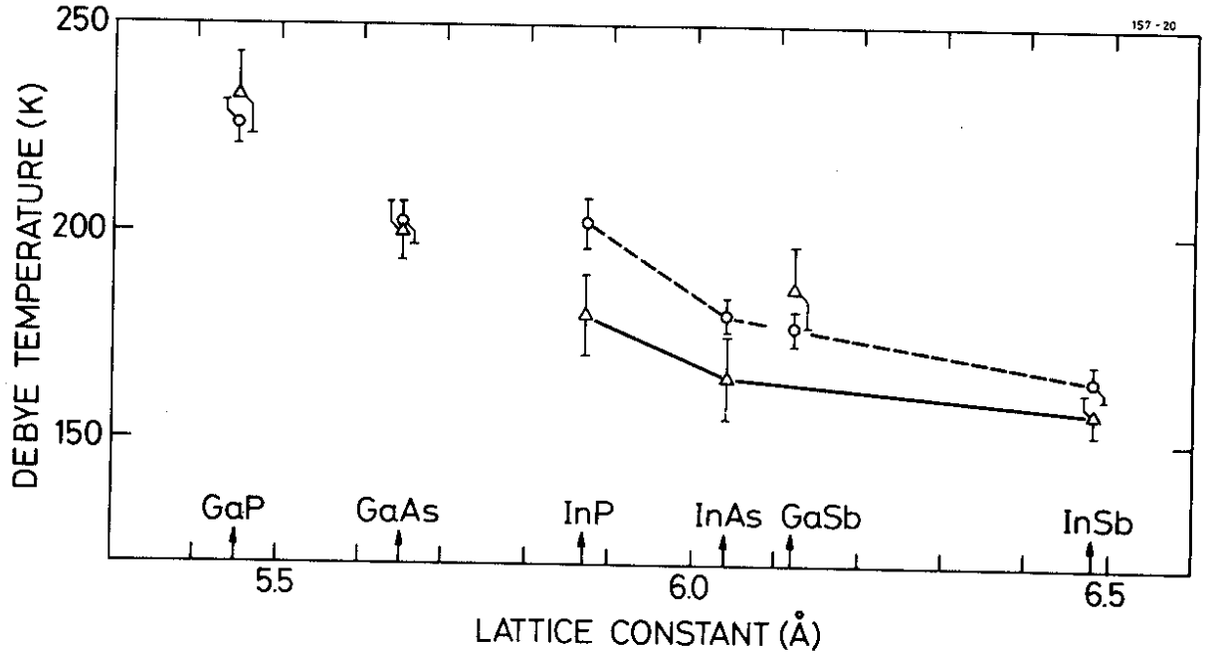
157 - 20
DEBYE TEMPERATURE (K)
250
200
150
GaP
GaAs
InP
InAs
GaSb
InSb
5.5
6.0
6.5
LATTICE CONSTANT (Å)

Fig. 4

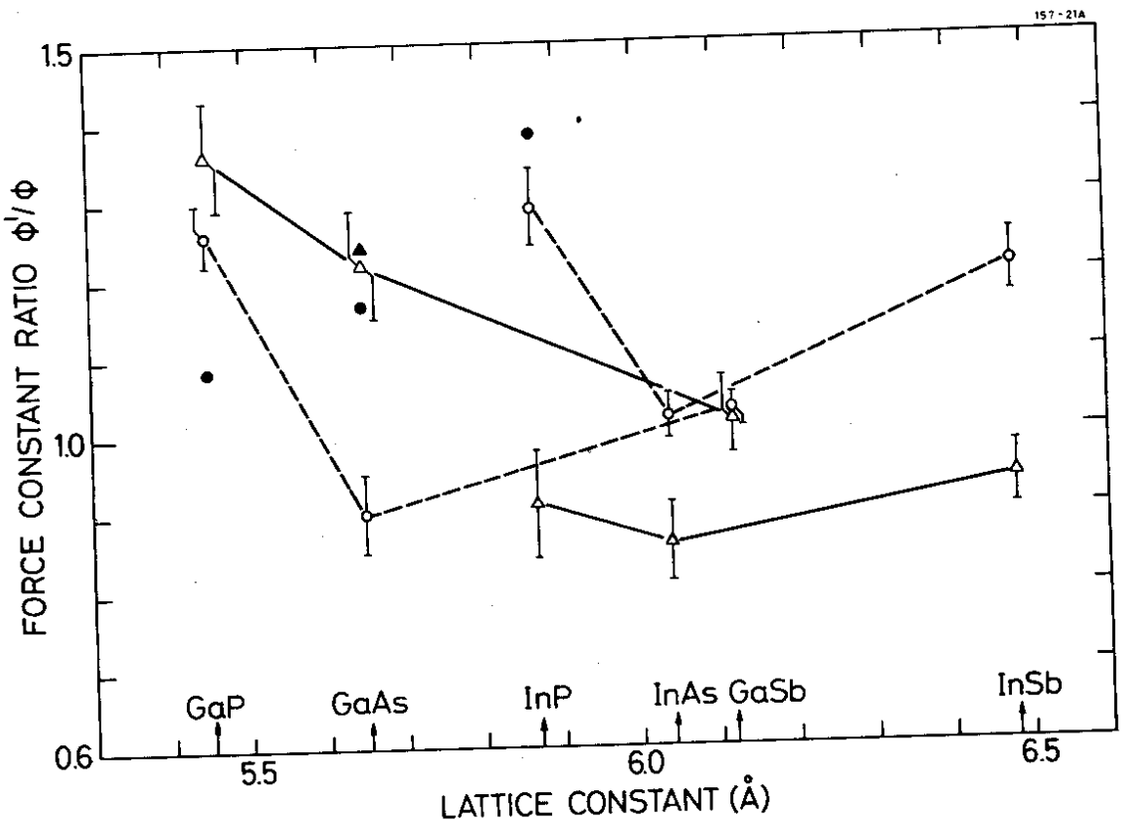
157-21A
1.5
1.0
0.6
FORCE CONSTANT RATIO φ'/φ
GaP
GaAs
InP
InAs GaSb
InSb
5.5
6.0
6.5
LATTICE CONSTANT (Å)

Fig. 5